JAEA-Technology
2007-014

JP0750151

JAEA-Technology

Operating Experiences since Rise-to-power Test in High Temperature Engineering Test Reactor (HTTR)

Daisuke TOCHIO, Shuji WATANABE
Toshihiro MOTEGI, Shuichi KAWANO
Yasuhiko KAMEYAMA, Kenji SEKITA
and Kozo KAWASAKI

Department of HTTR
Oarai Research and Development Center

March 2007

Japan Atomic Energy Agency | 日本原子力研究開発機構

本レポートは日本原子力研究開発機構が不定期に発行する成果報告書です。
本レポートの入手並びに著作権利用に関するお問い合わせは、下記あてにお問い合わせ下さい。
なお、本レポートの全文は日本原子力研究開発機構ホームページ（http://www.jaea.go.jp/index.shtml）より発信されています。このほか財団法人原子力弘済会資料センター*では実費による複写頒布を行っております。

〒319-1195　茨城県那珂郡東海村白方白根 2 番地 4
日本原子力研究開発機構　研究技術情報部　研究技術情報課
電話 029-282-6387, Fax 029-282-5920

*〒319-1195　茨城県那珂郡東海村白方白根 2 番地 4　日本原子力研究開発機構内

This report is issued irregularly by Japan Atomic Energy Agency
Inquiries about availability and/or copyright of this report should be addressed to
Intellectual Resources Section, Intellectual Resources Department,
Japan Atomic Energy Agency
2-4 Shirakata Shirane, Tokai-mura, Naka-gun, Ibaraki-ken 319-1195 Japan
Tel +81-29-282-6387, Fax +81-29-282-5920

JAEA-Technology 2007-014

Operating Experiences since Rise-to-power Test in High Temperature Engineering Test Reactor (HTTR)

Daisuke TOCHIO, Shuji WATANABE, Toshihiro MOTEGI, Shuichi KAWANO,
Yasuhiko KAMEYAMA, Kenji SEKITA and Kozo KAWASAKI

Department of HTTR
Oarai Research and Development Center
Japan Atomic Energy Agency
Oarai-machi, Higashiibaraki-gun, Ibaraki-ken

(Received January 18, 2007)

The rise-to-power test of the High Temperature Engineering Test Reactor (HTTR) was actually started in April 2000. The rated thermal power of 30MW and the rated reactor outlet coolant temperature of 850°C were achieved in the middle of Dec. 2001. After that, the reactor thermal power of 30MW and the reactor outlet coolant temperature of 950°C were achieved in the final rise-to-power test in April 2004. After receiving the operation licensing at 850°C, the safety demonstration tests have been conducted to demonstrate inherent safety features of the HTGRs as well as to obtain the core and plant transient data for validation of safety analysis codes and for establishment of safety design and evaluation technologies.

This paper summarizes the HTTR operating experiences for six years from start of the rise-to-power test that are categorized into (1) Operating experiences related to advanced gas-cooled reactor design, (2) Operating experiences for improvement of the performance, (3) Operating experiences due to fail of system and components.

Keywords : HTGR, HTTR, Operating Experience, Rise-to-power Test

高温工学試験研究炉 HTTR の
出力上昇試験からの運転経験

日本原子力研究開発機構大洗研究開発センター
高温工学試験研究炉部
栃尾　大輔、渡辺　周二、茂木　利広、河野　修一、亀山　恭彦、関田　健司、川崎　幸三

(2007 年 1 月 18 日受理)

高温工学試験研究炉（HTTR）では、2000 年 4 月より出力上昇試験を本格的に開始した。2001 年 12 月に HTTR の最大熱出力である原子炉熱出力 30MW 及び原子炉出口冷却材温度 850℃を達成した。その後、2004 年 4 月の最後の出力上昇試験において最大熱出力 30MW 及び原子炉出口冷却材温度 950°C を達成した。使用前検査合格証取得後は、高温ガス炉の安全解析コードの検証及び安全設計技術及び評価技術の向上を目的とした炉心及びプラントのデータを取得し、高温ガス炉固有の安全性を実証する安全性実証試験を行っている。

本報では、出力上昇試験開始から 6 年間の運転経験についてまとめている。これらについては、(1)新型のガス冷却炉設計に関連する運転経験、(2)性能向上のための運転経験、(3)系統や機器の故障等に関する運転経験、の 3 つに分類してまとめた。

大洗研究開発センター：〒311-1393　茨城県東茨城郡大洗町成田町 4002

Contents

目　次

1. Introduction

High Temperature Engineering Test Reactor (HTTR) which is the first High Temperature Gas-cooled Reactor (HTGR) in Japan was constructed at the Oarai Research and Development Center of Japan Atomic Energy Agency (JAEA) for the purpose of establishing and upgrading technologies of HTGRs as well as nuclear heat utilization. The first criticality of HTTR was achieved in November 1998. In March 2002, JAEA received a pre-operation test certificate, which is an operation license for HTTR in the rated operation mode (operation at a reactor-outlet coolant temperature of 850°C) from the government. After receiving the operation permit, the in-service operations have been conducted. A high-temperature test operation was started on March 2004, and reactor thermal power of 30MW and the reactor outlet coolant temperature of 950°C were achieved in April 2004[2]. The operation history of HTTR for six years from start of the rise-to-power test is shown in Fig. 1.1 and Table 1.1.

The structure and function of HTTR are differed from those of the other HTGRs like AVR of German HTGR. For example, pebble-bedded type fuels are used and the reactor outlet coolant temperature of 950°C was achieved in-vessel in AVR. On the other hand, block-type fuels are used and the reactor outlet coolant temperature of 950°C was achieved ex-vessel in HTTR

HTTR has three missions, (1) To establish HTGR technology like HTGR operation performance and demonstration of inherent safety feature, (2) To establish heat utilization system such as hydrogen production system, and (3) To establish high-temperature irradiation technology. The obtained data in HTTR operation will be useful for the safety design and evaluation technologies for the commercial HTGRs and the Very High-Temperature Reactor (VHTR). This report focuses on operating experiences for six years from start of the rise-to-power test in HTTR. Sections 2 and 3 provide HTTR history, HTTR design, and HTTR operating experiences.

Table 1.1 The HTTR operation history

Operation name	Operation mode	Max. thermal power (MW)	Duration	Operation time (MWd)
1st phase rise-to-power test (PT-1)	RS/RP	9	2000 4/23 - 5/8 2000 5/11 - 5/26 2000 5/30 - 6/6	193
2nd phase rise-to-power test (PT-2)	RS/RP	20	2000 7/3 - 7/8*1 2001 1/29 - 2/12 2001 2/16 - 3/1	486
3rd phase rise-to-power test (PT-3)	HS/HP	20	2001 4/14 - 5/7 20015/11 - 5/16*2 2001 5/21 - 6/8	689
4th phase rise-to-power test (PT-4)	RS/RP	30	2001 10/23 - 12/14 2002 1/25 - 3/6	2277
1st operation cycle	RP/RS-1	30/9	2002 5/30 - 6/17 2002 6/21 - 7/1	462
2nd operation cycle	RS-2	30	2003 2/5 – 3/14	658
3rd operation cycle	RP-3	20	2003 5/16 - 5/21*1	72
4th operation cycle	RS-4	9	2003 8/8 - 8/11	25
5th operation cycle	RS-5	30/8	2004 1/27 - 2/25 2004 2/29 - 3/5	549
5th phase rise-to-power test (PT-5)	HS/HP	30/30	2004 3/31 - 5/1 2004 6/2 - 7/2	1305
6th operation cycle	RS-6	9	2005 2/14 - 2/19 *3	0.95
7th operation cycle	RS-7	27.6	2005 8/30 - 9/12*2	206

R: Rated operation S: Single loaded operation mode

H: High temperature operation mode P: Parallel loaded operation mode

*1: Automatic reactor scram caused by a signal of the PPWC flow-rate low

*2: Automatic reactor scram caused by a loss of off-site electric power

*3: Automatic reactor scram caused by a malfunction

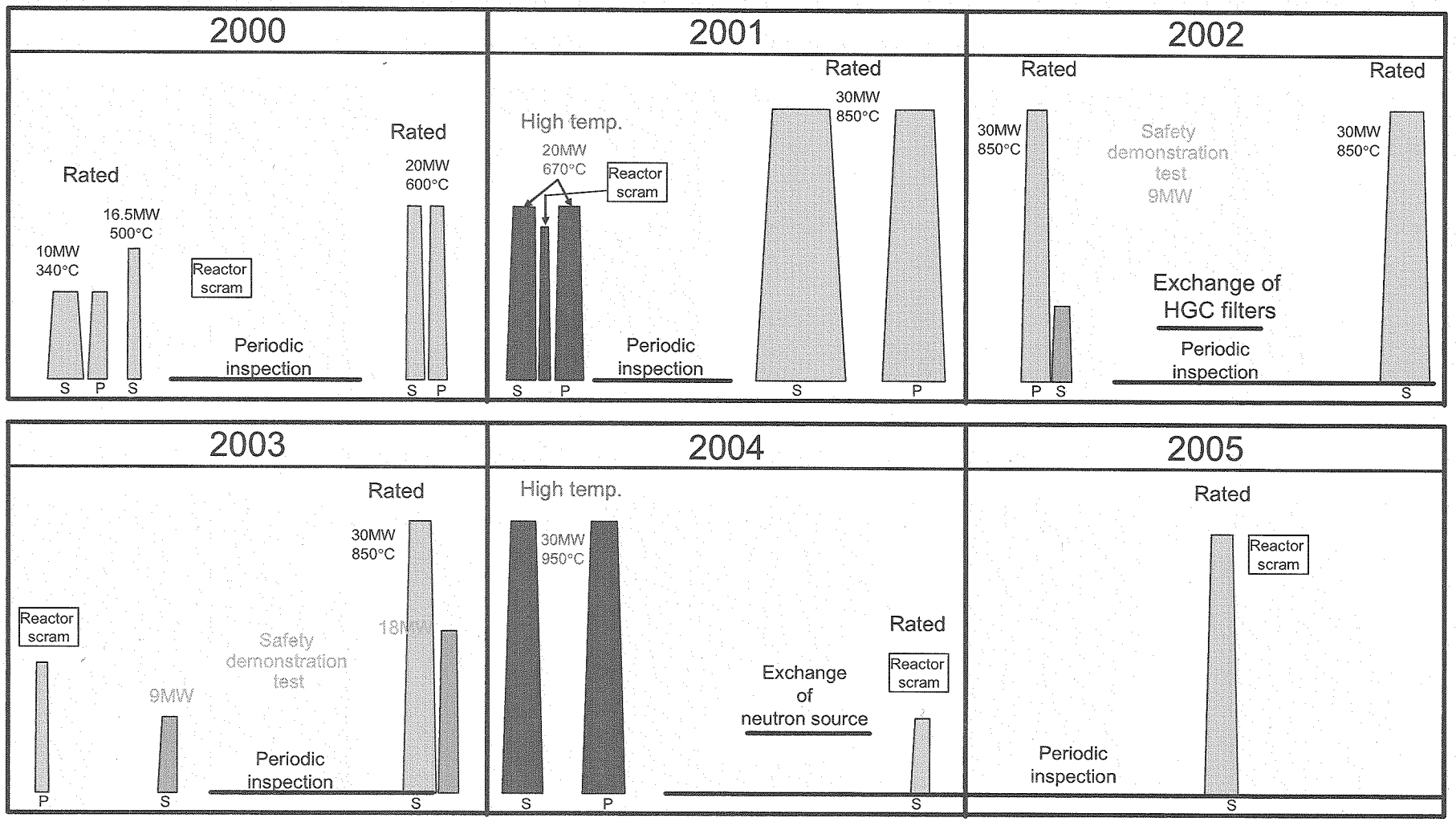

Rated: Rated operation mode
S: Single-loaded operation
High temp.: High temperature test operation mode
P: Parallel-loaded operation

Fig. 1.1 The HTTR operation history for six years from start of the rise-to-power test

2. Outline of HTTR

2.1 History of HTTR

HTGR development history in JAEA started from 1960s. At that time, the possibility of direct steel manufacturing by utilizing heat from HTGR was searched for. Then VHTR project with reactor outlet temperature of 1000 °C was initiated in 1969 at JAEA, including research and development (R&D) which covers all fields necessary for the reactor design and construction of the VHTR. However, there was no urgent or commercial demand coming up afterwards, although the essential needs of HTGR were well understood for the future.

Thus, the project was reviewed by the government to shift to more basic research for the future rather than immediate development of commercial reactors. In accordance with this review, the Atomic Energy Commission of Japan issued the revision of long-term program for research, development and utilization of nuclear energy in 1987, recommending that Japan should proceed with the development of more advanced technologies for the future, in parallel with existing nuclear systems. The long-term program emphasized that HTGR is considered as one of the most promising nuclear reactors to improve the economy and enhance the application of nuclear energy.

The Japan Atomic Energy Commission decided to construct HTTR. The mission of HTTR is as follows:

- To establish HTGR technology like as upgrade of HTGR operation performance and demonstration of inherent safety feature
- To establish heat utilization system like as hydrogen production system
- To establish high-temperature irradiation technology

The construction of HTTR was initiated in 1991, the rise-to-power test was started in 1999 and the operation license of HTTR was issued on March 6, 2002 from the Ministry of Education, Culture, Sports, Science and Technology (MEXT). We started extensive tests using HTTR. The maximum reactor outlet coolant temperature of 950°C was achieved in April 2004, and the operation license of HTTR was issued in June 2004 from MEXT.

The above-mentioned history of HTTR Project is summarized in Fig. 2.1.

2.2 Outline of HTTR[3)]

Bird's-eye view of HTTR facility is shown in Fig. 2.2 and the major specifications of HTTR are summarized in Table 2.1. The reactor core is designed to generate thermal power of 30MW and consists of array of hexagonal graphite fuel assemblies so-called "pin-in-block type fuel", control rods, graphite reflectors etc.

2.2.1 Reactor

The structural diagram of HTTR fuels is shown in Fig. 2.3. A fuel block consists of 31 or 33 fuel rods and a hexagonal graphite block, 360mm across flats and 580mm in height. Fuel assembly has three dowel pins on the top and three mating sockets at the bottom to align the fuel assemblies. Tri-isotropic (TRISO)-coated fuel particles with UO_2 kernel, about 6wt% average enrichment and 600μm in diameter, are dispersed in the graphite matrix and sintered to form a fuel compact. Fourteen fuel compacts are contained in a fuel rod, 34mm in o. d. and 577mm in length. Fuel rods are inserted into vertical holes in the graphite block. Coolant of helium gas flows through gaps between the holes and the rods.

In the safety design of HTGR fuels, it is important to retain fission products within particles so that their release to the primary coolant may not exceed an acceptance level. From this point of view, the basic design criteria for the fuel are as follows: (1) to minimize the failure fraction of as-fabricated fuel coating layers, (2) to avoid significant additional fuel failures during operation. To satisfy the latter criteria for the first loading fuel, the fuel temperature is limited to below 1495°C under a normal operation condition and below 1600°C under an abnormal transient condition.

The arrangement of core components and core internals are shown in Fig. 2.4. One column is the pile of prismatic hexagonal blocks piled up axially. The active core (2.9m in height and 2.3m in diameter) consists of 30 fuel columns and 7 control rod (CR) guide columns, and that is surrounded by 12 replaceable reflector columns, 9 reflector region CR guide columns and 3 irradiation test columns.

Reactor internals consist of graphite and metallic core support structures and shielding blocks. They support and arrange the core components, such as fuel assembly and replaceable reflector blocks, within the reactor pressure vessel (RPV). The graphite core support structure consists of permanent reflector blocks, hot plenum blocks, support posts, core bottom structures and so on. The metallic core support structures consist of support plates, a support grid, core restraint mechanism and so on.

Reactivity is controlled by CRs as shown in Fig. 2.5. The CRs are individually supported by control rod drive mechanism located in the standpipes connected to the RPV hemispherical top lid. The reactor is shut down at first by inserting 9 pairs of CRs into the reflector region. After the temperature decreases, the rest 7 pairs of the CRs are inserted into the active core region. This is the reason that the CRs do not exceed their design

temperature limit.

Figure 2.6 shows the schematic diagram of Reserved Shutdown System (RSS) used in the HTTR. The RSS is located in the stand-pipes accompanied by the CR system. In case CRs fail to be inserted, the RSS drops boron-carbon/carbon (B_4C/C) pellets into the core to shut down the reactor. The RSS consists of B_4C/C pellets, hoppers which contain the pellets, driving mechanisms, guide tube and so on.

In accidents when the CRs cannot be inserted, an electric plug is pulled out by a motor and the absorber pellets fall into the core by gravity.

2.2.2 Reactor Cooling System

Reactor cooling system is composed of a main cooling system (MCS), an auxiliary cooling system (ACS) and a vessel cooling system (VCS) as shown in Fig. 2.7.

MCS is operated in normal operation to remove heat from the core and transfer it to the environment via intermediate heat exchanger (IHX) of 10MW and primary pressurized water cooler (PPWC) of 20MW in parallel, called parallel loaded operation, or via only PPWC of 30MW, called single loaded operation. The primary coolant gas comes into the reactor pressure vessel (RPV) at 395°C, and heated up to 850°C at the reactor outlet at the rated operation mode and 950°C at high temperature test operation mode.

ACS is designed as an engineered safety feature to operate upon a reactor scram and cool down the core and the core support structure. On the other hand, VCS cools the biological shield of concrete in normal operation and acts as a cooling system upon postulated accidents such as loss of forced convection cooling, e.g. the rupture of primary concentric hot gas duct. Decay heat and residual heat removed by the heat transfer (largely by radiation) from RPV to the cooling panel of VCS.

2.2.3 Instrumentation and Control System

Instrumentation and the control system consist of the instrumentation, control, safety protection systems as well as a control room. The instrumentation system consists of nuclear instrumentation, in-core temperature monitoring and fuel failure detection reactor systems.

The nuclear instrumentation system of HTTR is composed of the wide range monitoring system (WRMS) and the power range monitoring system (PRMS) as shown in Fig. 2.8. WRMS is used to measure the neutron flux from 10^{-8}% to 30% of the rated power. Three fission chambers are installed in the permanent reflector blocks through the standpipe. PRMS is used to measure the neutron flux from 0.1% to 120% of the rated power. PRMS is also used as the sensor for the reactor power control system. It is difficult to monitor the reactor core because the temperature and neutron flux level in RPV are very high in full power operation. The detector of PRMS is required to be located outside RPV because

available working temperature of PRMS is very lower than coolant temperature.

In order to monitor the core outlet coolant temperature, seven thermocouples (T/Cs) are arranged at the hot plenum blocks below the reactor core. The N-type T/C (Nicrosil-Nisil) is selected because the primary coolant temperature in the hot plenum reaches about 1,000°C at the rated power operation.

The fuel failure detection system is composed of precipitators, a pre-amp, and a control box and so on. The precipitator is used for the purpose of detection of ß rays radiated from the short-lived gaseous fission products such as Krypton-88 (^{88}Kr) and Xenon-138 (Xe-138) released from the failed fuel particles.

The reactor control system is designed to assure high stability and reasonably damped characteristics against the various disturbances during the operation. The main control system of HTTR consists of the operation mode selector, reactor power control system and plant control system. Operation mode selector is designed to select several mode operations such as the rated power operation, the high temperature test operation, the safety demonstration test operation and so on. The reactor power control system consists of the power control devices and reactor outlet coolant temperature control device. The reactor outlet coolant temperature control device is an upper one to give demand of reactor power to the power control device.

Safety protection system consists of the reactor protection system and engineered safety features actuating system. It is designed with 2-out-of-3 circuit logic with 2-trains. The reactor protection system of HTTR automatically initiates a reactor scram by inserting the CRs. Engineered safety features actuating system of HTTR is designed to restrain the release of the fission product and to ensure the integrity of the core, the reactor coolant pressure vessel boundary against unexpected conditions during abnormal operational transients and accidents.

Table 2.1 Major specification of HTTR

Thermal power	30MW
Outlet coolant temperature	850°C/950°C
Inlet coolant temperature	395°C
Fuel	Low enriched UO_2
Fuel element type	Prismatic block
Direction of coolant flow	Downward
Pressure vessel	Steel
Number of cooling loop	1
Heat removal	IHX and PPWC
Primary coolant pressure	4MPa
Containment type	Steel containment
Plant lifetime	20 years

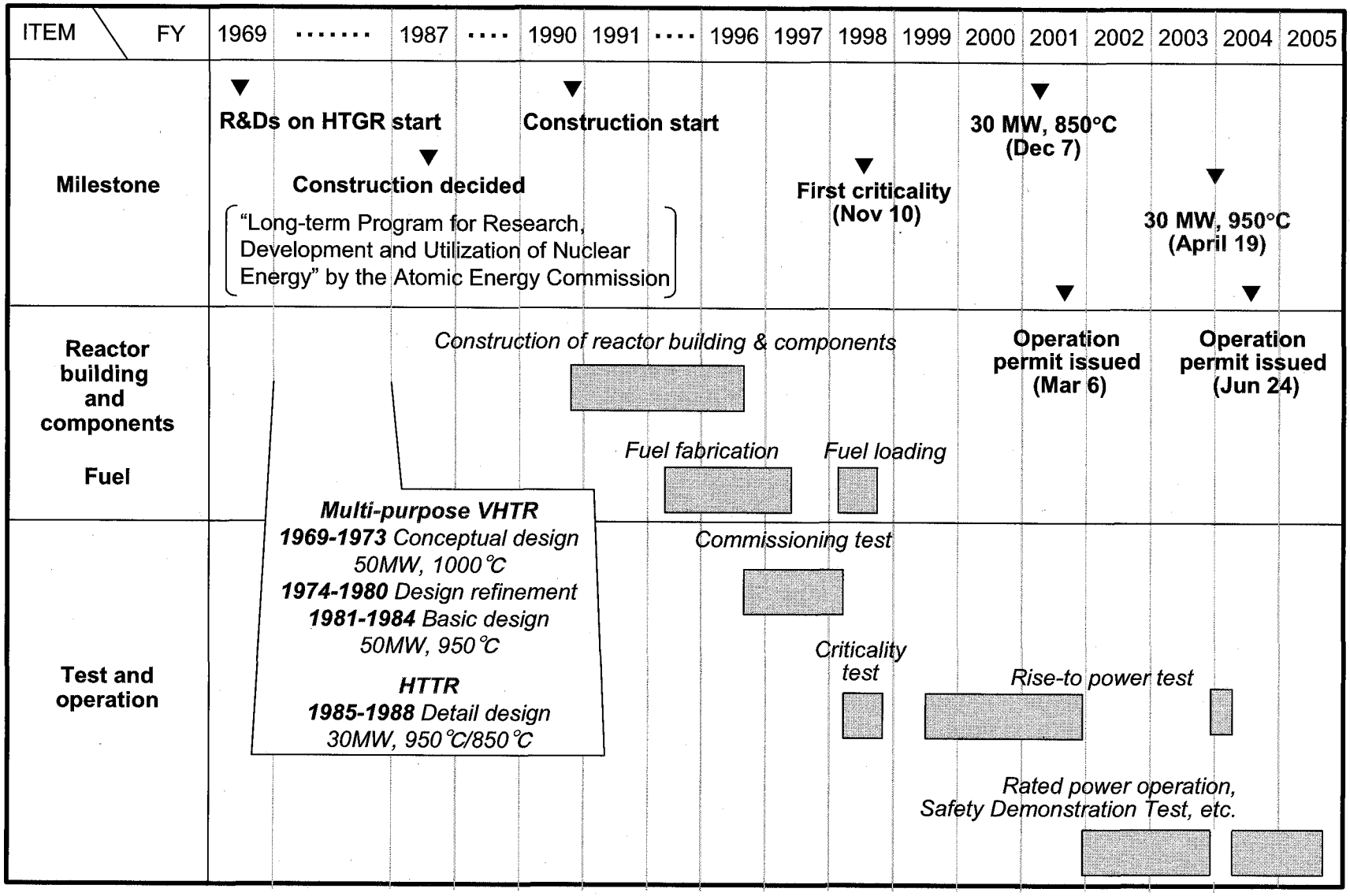

Fig. 2.1 History of HTTR project

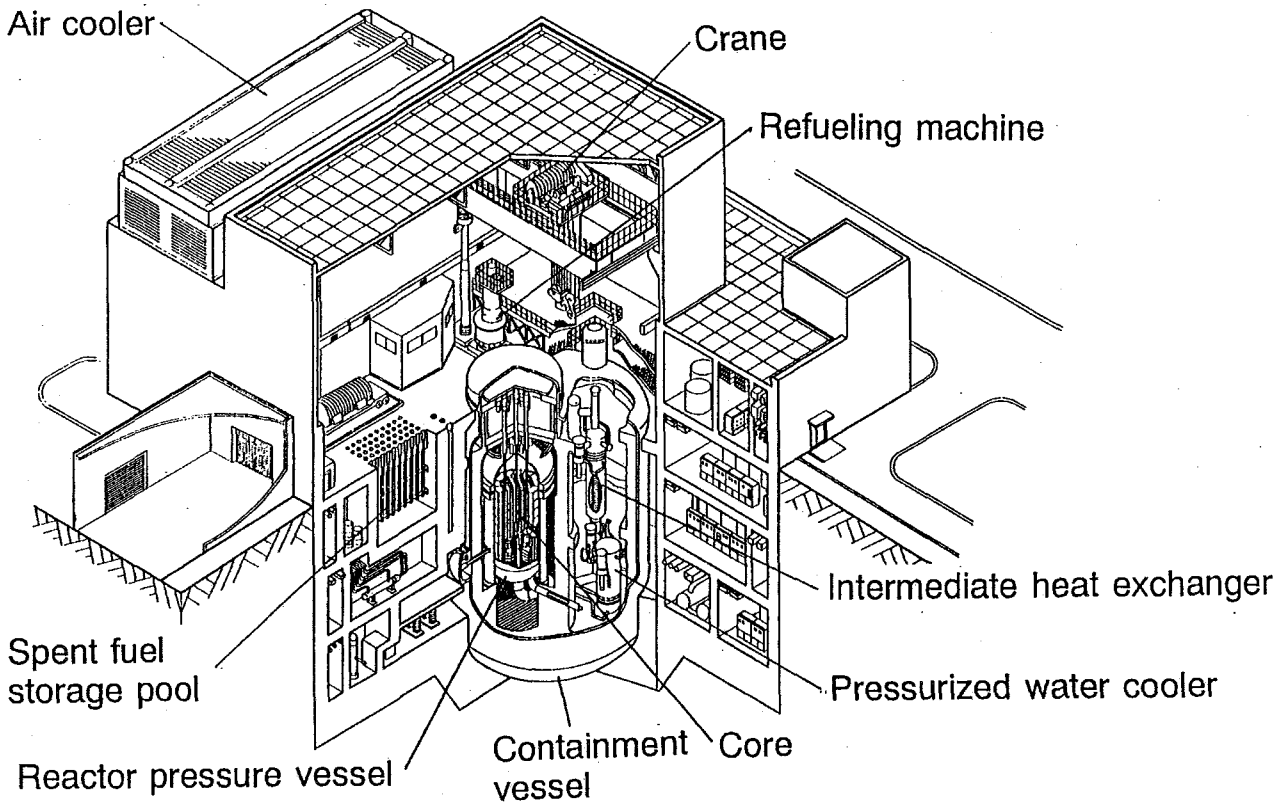

Fig.2.2 Bird's eye view of HTTR facility

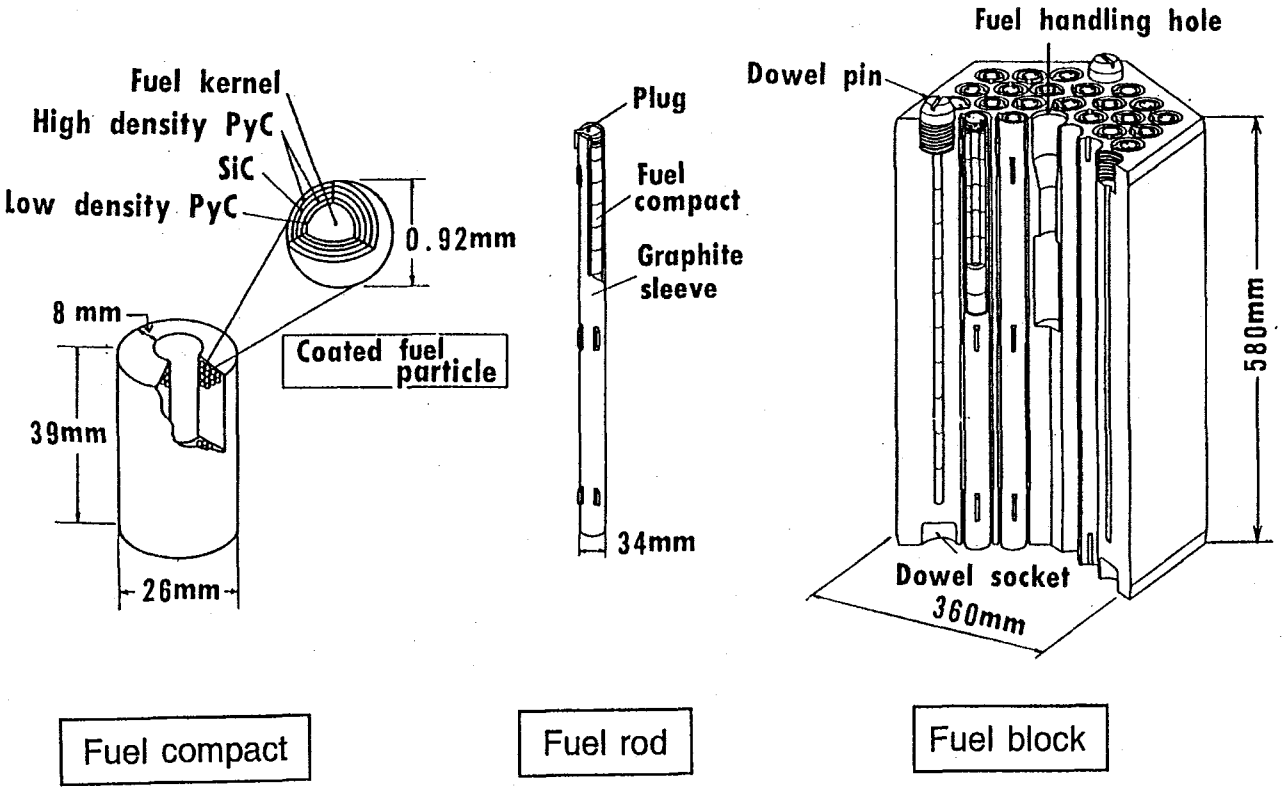

Fig. 2.3 HTTR fuels

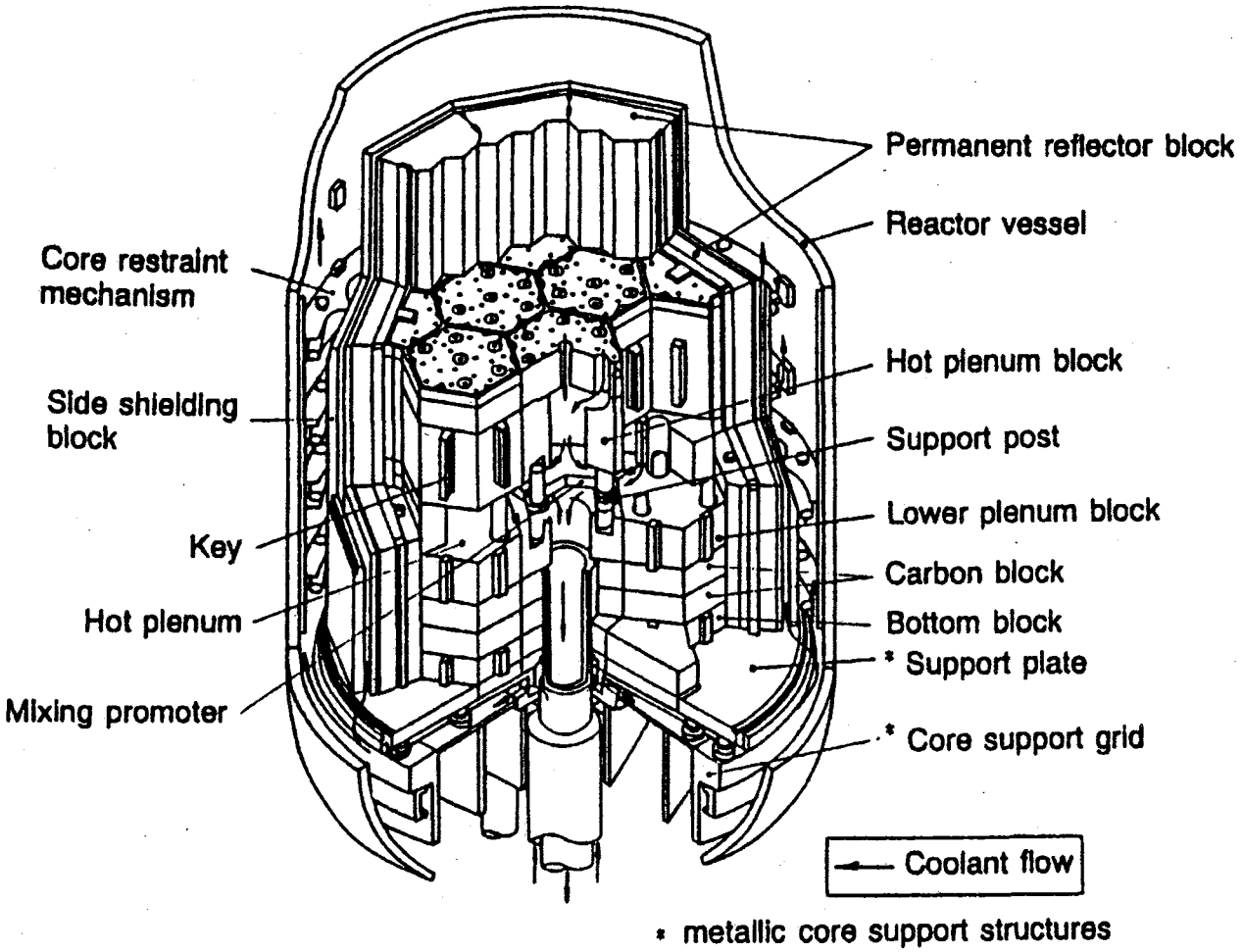

Fig. 2.4 Core support structures of HTTR.

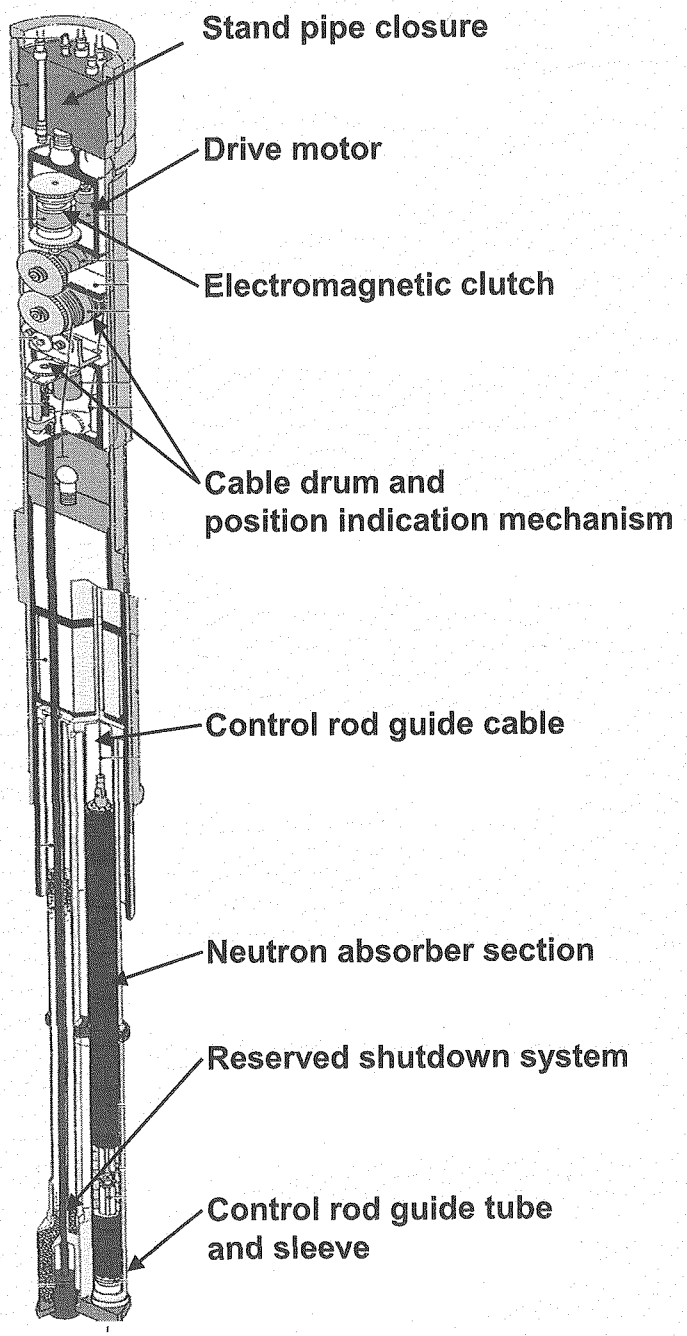

Fig.2.5 Cross-sectional view of the control rod driving unit

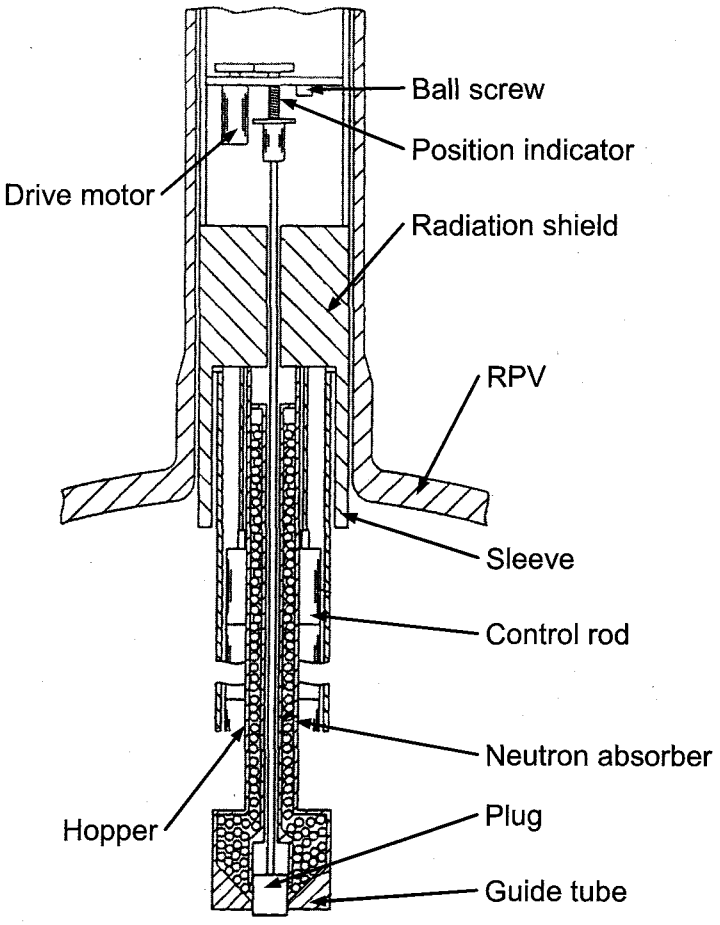

Fig. 2.6 Schematic diagram of reserved shutdown system

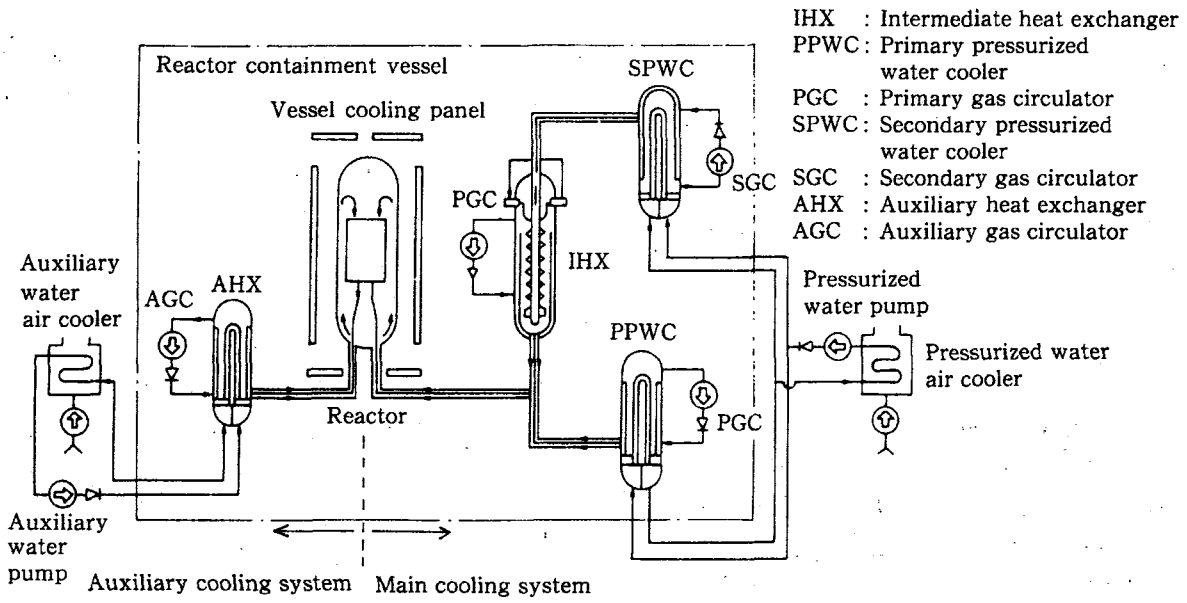

Fig. 2.7 The HTTR cooling system

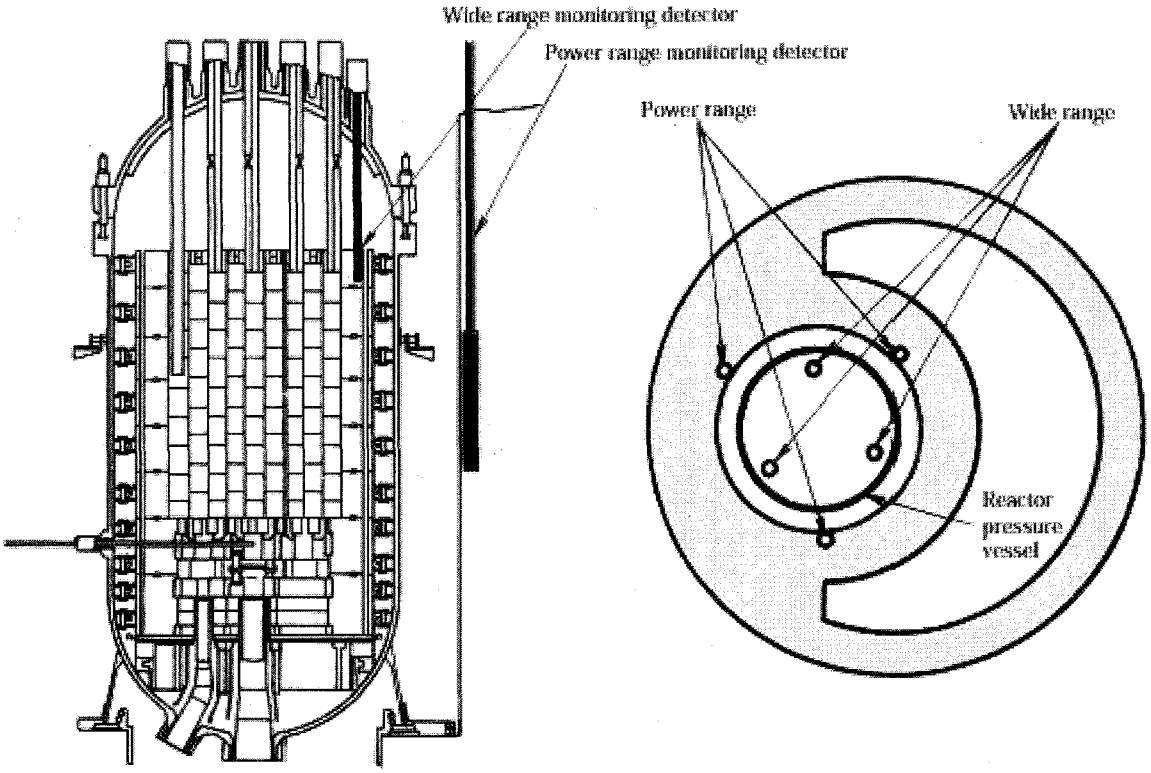

Fig. 2.8 The arrangement of the neutron detectors

3. Operating experiences for six years from start of the rise-to-power test

The operating experiences for six years from start of the rise-to-power test are divided into three categories:

(1) The operating experiences that contribute to design of the next generation HTGR include the helium handling techniques, the helium impurity control, the helium gap flow for block typed core, the fission product gases behavior and the confirmation of fuel integrity.

(2) The operating experiences for improvement of the performance of HTTR include the filter exchange of the primary gas circulator (PGC), installation of the windshield panels to improve the air-cooler performance the failure in monthly movement test of Reactor Shutdown System (RSS), and the contact failure of signal lead wire in WRM.

(3) The operating experiences on failure of system and components include the reactor scrams and countermeasures that had been made for re-start.

3.1 Operating experiences that contribute to design of the next generation HTGR

3.1.1 Helium leak rate from the main cooling system[1),2)]

It is important to restrict the helium leakage of the main cooling system from the viewpoint of preventing the release of radioactive materials and confirming the integrity of the pressure boundary. Just before the power up of HTTR after each periodic inspection, the helium leak rate from the main cooling system was measured under the pressure of 4MPa, which is operation pressure at full power.

Table 3.1 summarizes the measured leak rates from 2000 to 2005. In HTTR, the helium leak rate is measured with pressure drop method. The measured leak rates were much smaller than the limit of 0.3%/day.

Table3.1 Measured helium leak rate

	Result (%/day)	Remarks
1st phase rise to power test(PT-1)	0.06	
2nd phase rise to power test(PT-2)	0.16	
3rd phase rise to power test(PT-3)	0.05	
4 th phase rise to power test(PT-4)	0.16	Achievement of 850°C at 30MW
1st operation cycle(RS-1)	0.16	
2nd operation cycle(RS-2)	0.12	
3rd operation cycle(RS-3)	0.10	
4th operation cycle(RS-4)	0.06	
5 th operation cycle(RS-5)	0.13	
5 th phase rise to power test(PT-5)	0.15	Achievement of 950°C at 30MW
6th operation cycle(RS-6)	0.07	
7th operation cycle(RS-7)	0.18	

3.1.2 Coolant chemistry[1),2)]

The coolant chemistry control is important because the impurities cause oxidation of the graphite used in the core and the corrosion of the high-temperature metallic materials used in the heat exchanger, etc. The coolant chemistry is monitored by the helium sampling system continuously during the operation. The chemical impurities of carbon monoxide (CO), hydrogen (H_2), carbon dioxide (CO_2), water vapor (H_2O(g)), methane (CH_4), nitrogen (N_2), oxygen (O_2), etc. are removed by the helium purification system. The each impurity concentration was severely limited by the operating manual during the operation.

Figure 3.1 shows the chemical impurity behavior during the single-loaded and high-temperature test operation. The each impurity was steadily removed by the purification system. In the operations below 850°C, which had been previously performed, the impurities did not increase rapidly. After the temperature rose from 850°C, the impurities of H_2, CO, CO_2 and N_2 increased rapidly, and small amounts of CH_4 and O_2 were detected. The following two reasons are considered: The one is the impurity release from the graphite component in the core and insulator in the concentric hot gas duct. The other is the chemical equilibrium in the core. The H_2O(g), which was emitted from the graphite, converted to H_2 and CO by an immediate reaction in the high-temperature conditions in the core. Therefore, the behavior of H_2 and CO were very similar to that of H_2O(g) especially after the power up from 850°C.

The primary coolant impurity limits of HTTR, chemical impurity at reactor outlet coolant temperature of 850°C and 950°C are shown in Table 3.2.

Table 3.2 The primary coolant impurity concentration

	H_2	CO	H_2O	CO_2	CH_4	N_2	O_2
Impurity limit (above 800°C of reactor-outlet coolant temp.)	3.0	3.0	0.2	0.6	0.5	0.2	0.04
Rated op. (850°C @2000/12/14)	0.62	0.62	0.12	0.13	0.05	0.10	0.01
High temp. test op. (950°C @2004/4/19)	0.21	1.32	0.08	0.19	0.01	0.15	0.03

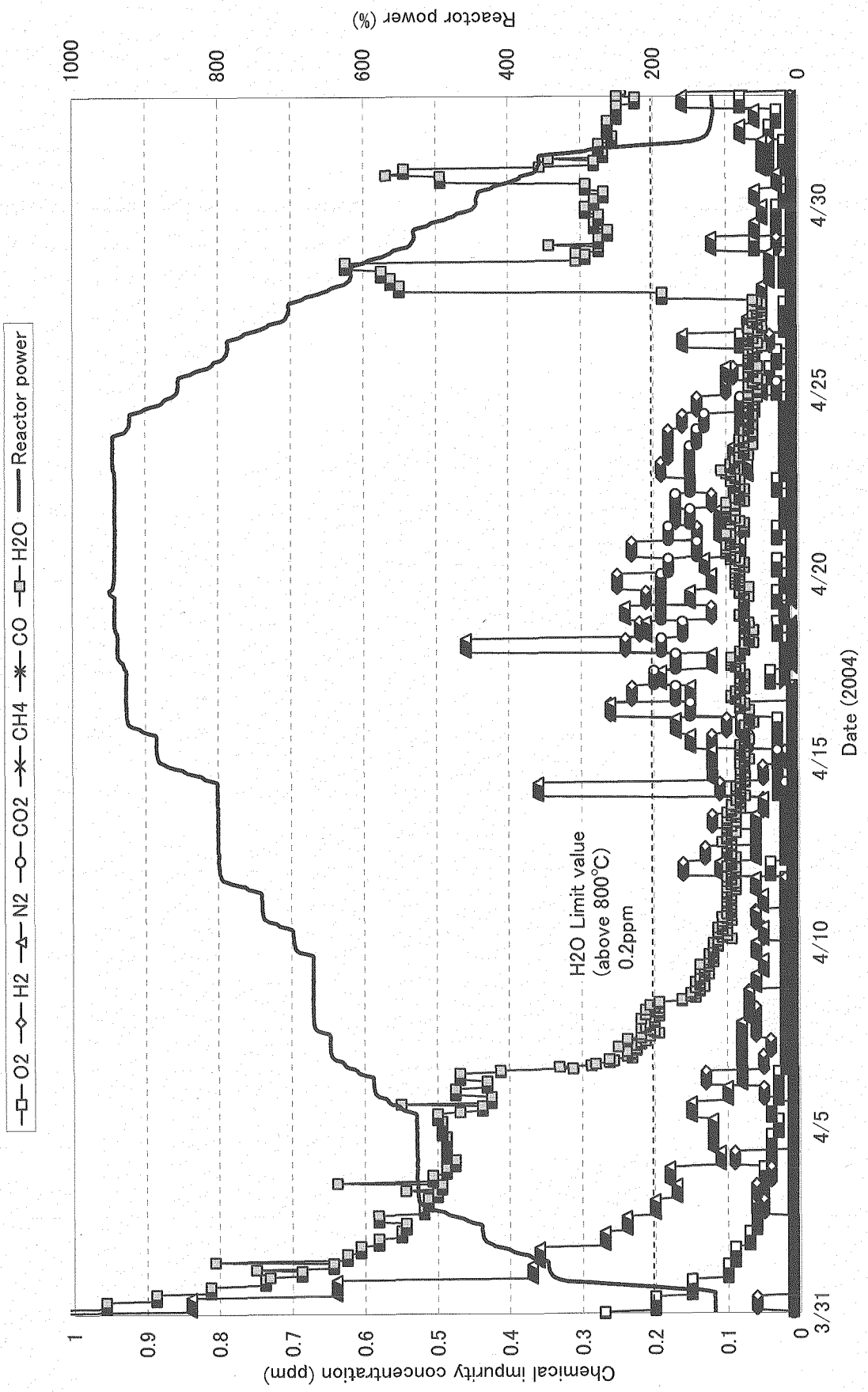

Fig. 3.1 The time variation of chemical impurity in high-temperature test operation mode

3.1.3 Core support plate temperature rise[6)]

In the 2nd phase rise-to-power test at rated operation mode, the core support plate temperature at center became much higher than the predicted one. By the linear extrapolation of the test data (see Fig. 3.2), the temperature at full power, that is, at the reactor outlet coolant temperature of 850°C was expected about 470°C that is the design working temperature of the core support plate. To investigate the cause of the temperature rising, the 3rd phase rise-to-power test to 20 MW at high temperature test operation mode was conducted. The test result at the high temperature test operation mode is also shown in Fig. 3.2, in which the core support plate temperature at full power, that is, at the reactor outlet coolant temperature of 950°C, was predicted to be about 450°C.

The analytical calculation of the core support plate temperature using FEM code ANSYS was performed. As the result, we concluded that the cause of the temperature rise is the "Gap flow". The "Gap flow" is the flow of hot helium gas through gaps between core support graphite blocks induced by pressure difference between the hot plenum and inside of the primary helium gas duct as shown in Fig. 3.3. The "Gap flow" was estimated to be an order of 10 g/s. It flows downward from the hot plenum through the gaps between lower plenum blocks, carbon blocks, bottom blocks, and core support plates. And it goes horizontally between the core support plates and a seal plate, goes upward along the outside of the primary helium gas duct, and then flows into the primary helium gas duct.

Because it is impossible to approach and modify the core support structure, the design temperature was revised. In order to confirm the integrity of structure, structure integrity analysis was performed. As the result, changeable design temperature of 530°C was obtained. So the design temperature was changed from 470°C to 530°C.

After the revision of the design temperature, the 4th and 5th phase rise-to-power test were preformed. Figure 3.4 shows the measured result of core support plate temperature in the 4th and 5th phase rise-to-power test. It was confirmed that measured temperature was almost the same as the predicted values shown in Fig. 3.2 and that the measured temperature did not exceed the design temperature.

The core support structure was designed based on previous experimental data obtained in the Helium Engineering Demonstration Loop (HENDEL). However the unexpected distortion of the seal plate due to core pressure difference was generated. So the flow distribution was changed from expected one. As the result, core support plate temperature was raised. This phenomenon was not expected in the reactor design of HTTR, and it is an important operational experience for future HTGR design.

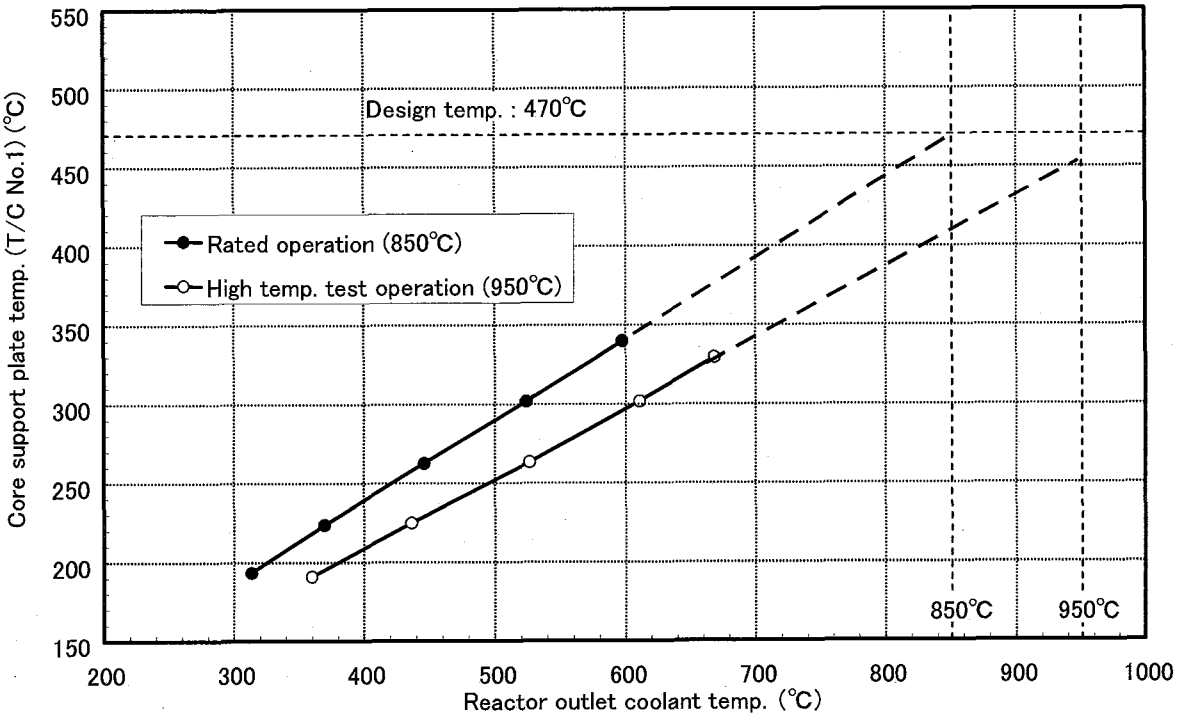

Fig. 3.2 The measured core support plate temperature in the 2nd phase rise-to-power test

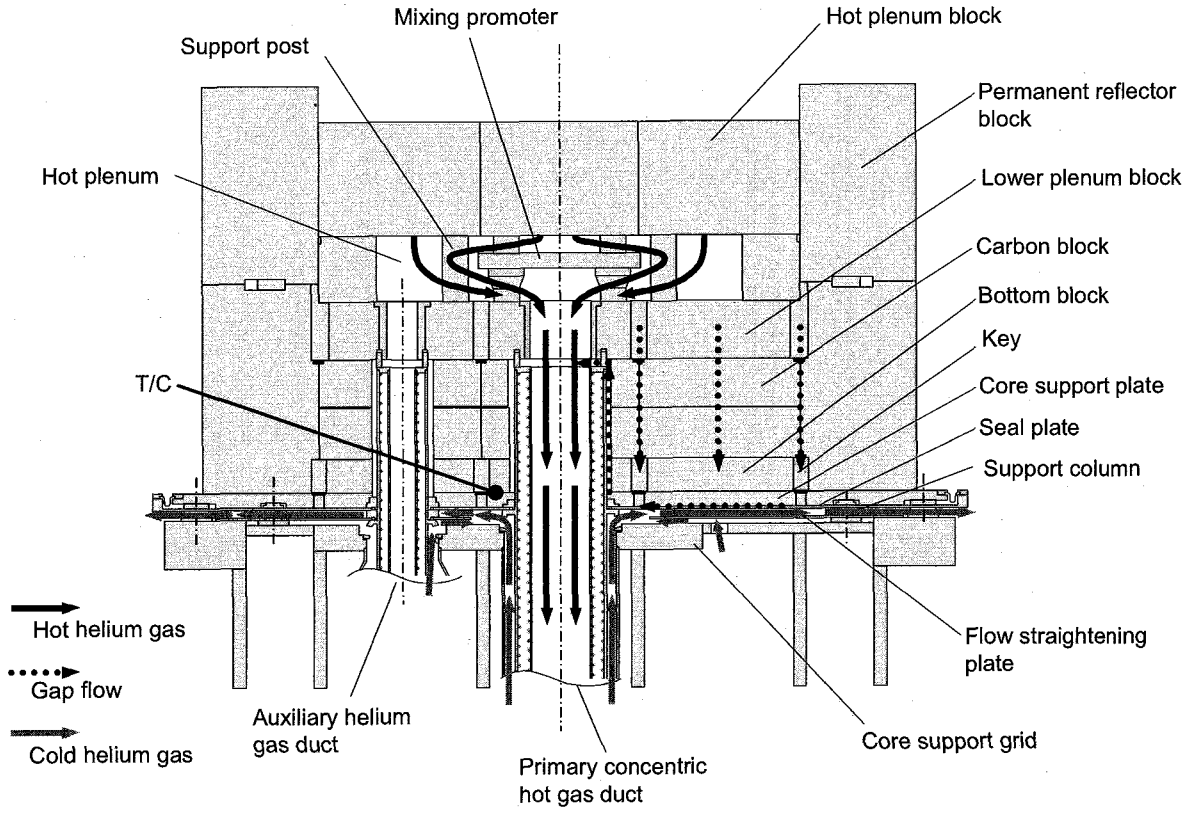

Fig. 3.3 The gap flow in core support structure

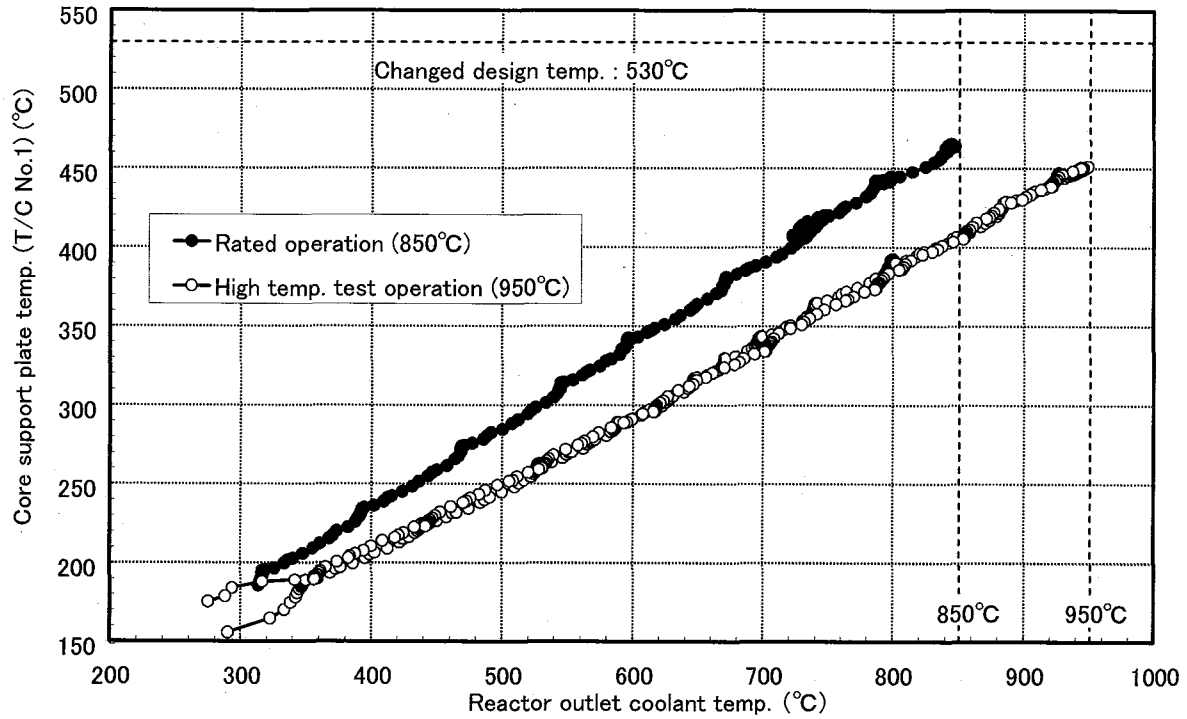

Fig. 3.4 The measured core support plate temperature in the 4th and 5th phase rise-to-power test

3.1.4 Fuel and fission product gas behaviors[4)]

In order to evaluate the fission product gas release behavior and to confirm that the released fission product gas levels were within their limits during the operation, the fuel and fission product gases behavior was monitored. The primary coolant radioactivity instrumentation of the safety protection system, the Fuel Failure Detection (FFD) system, and the primary coolant sampling system are installed in the primary circuit in order to measure the primary coolant radioactivity.

The primary coolant radioactivity was measured continuously during the operation as shown in Fig. 3.5. All signals were less than the alarm level of 10GBq/m^3 which corresponds to the 0.2% fuel failure. Moreover, all signals were less than the detection limit (1GBq/m^3).

The FFD system are employed in HTTR to detect the additional abnormal failure of the coated fuel particles during the normal operations. **Figure 3.6** shows the FFD signal during the operation. The signal varied in proportion to the reactor power, which increased linearly up to the reactor power of 60% and exponentially thereafter. Over the reactor power of 60%, the FFD signal values in high-temperature test operation were higher than those in rated operation.

The primary coolant sampling measurement is the only way to determine the fission product gas concentrations. As the results, the detected fission gas nuclides in the primary coolant were krypton-85 metastable (^{85m}Kr), krypton-87 (^{87}Kr), krypton-88 (^{88}Kr), xenon-133 (^{133}Xe), xenon-135 (^{135}Xe), xenon-135 metastable (^{135m}Xe), and xenon-138 (^{138}Xe), all of which are the same isotopes as those for previous tests in rated operation mode. The measured release-birth rate (R/B rate), of ^{88}Kr as a function of the reactor power are plotted in Fig. 3.7. In the operation, the measured fractional release at 50% of the reactor power showed the same levels as those in rated operation mode, and then increased exponentially to 1.0×10^{-8} at the full power operation, which was slightly larger than 7×10^{-9} in the rated operation mode,.

The measured R/B at the full power was three orders lower than the limitation of 5.35×10^{-4}, which corresponds to 1% fuel failure. It suggests that the measured values were within the release level by diffusion of the generated fission gas from the contaminated uranium in the fuel compact matrix, and no significant failure occurred during 950°C operation.

In HTTR, the primary coolant radioactivity is very low (correspond to 0.01% fuel failure) in normal operation. The public dose rate is very lower than that limit value at the occurrence of Design Basis Accident (DBA) even if all the radioactive materials in the coolant are released to the ground.

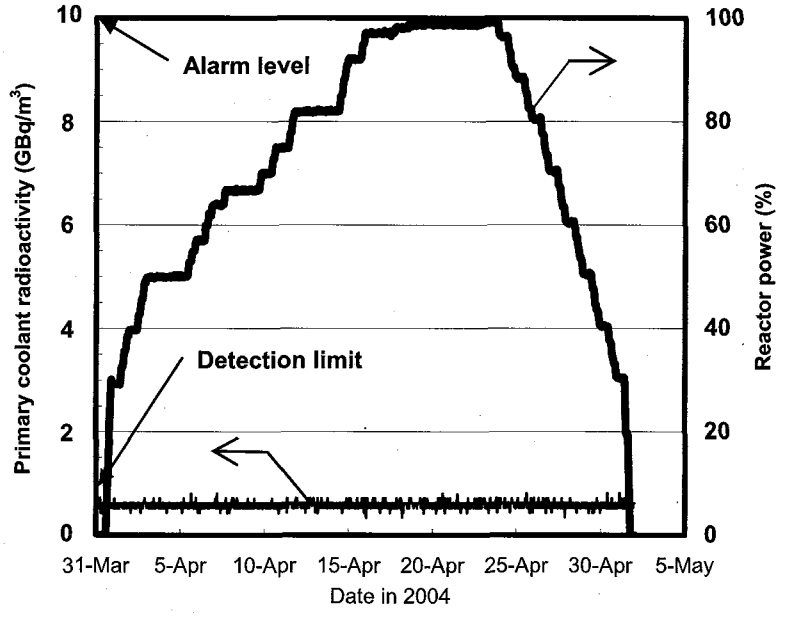

Fig. 3.5 The time variation of primary coolant radioactivity

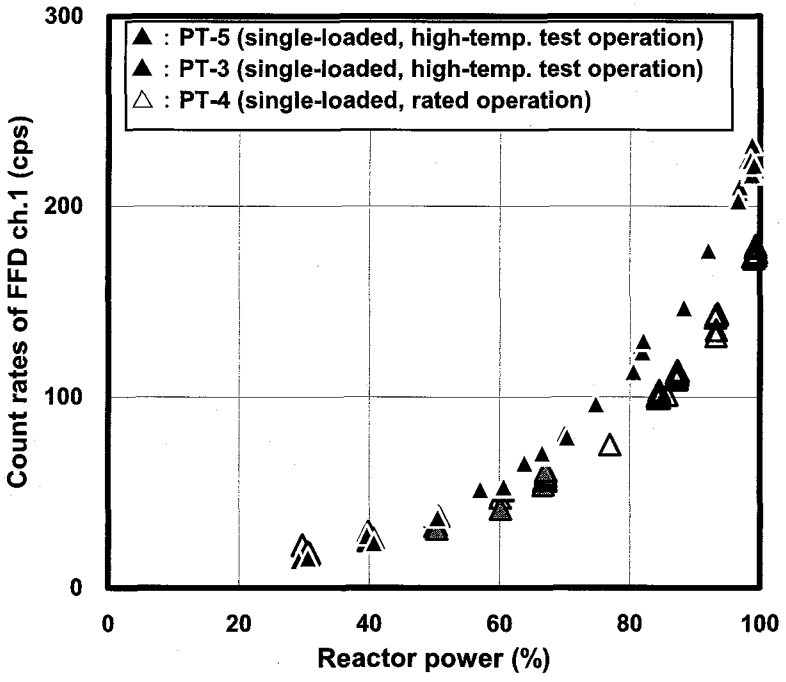

Fig. 3.6 The relationship between FFD count rates and reactor power

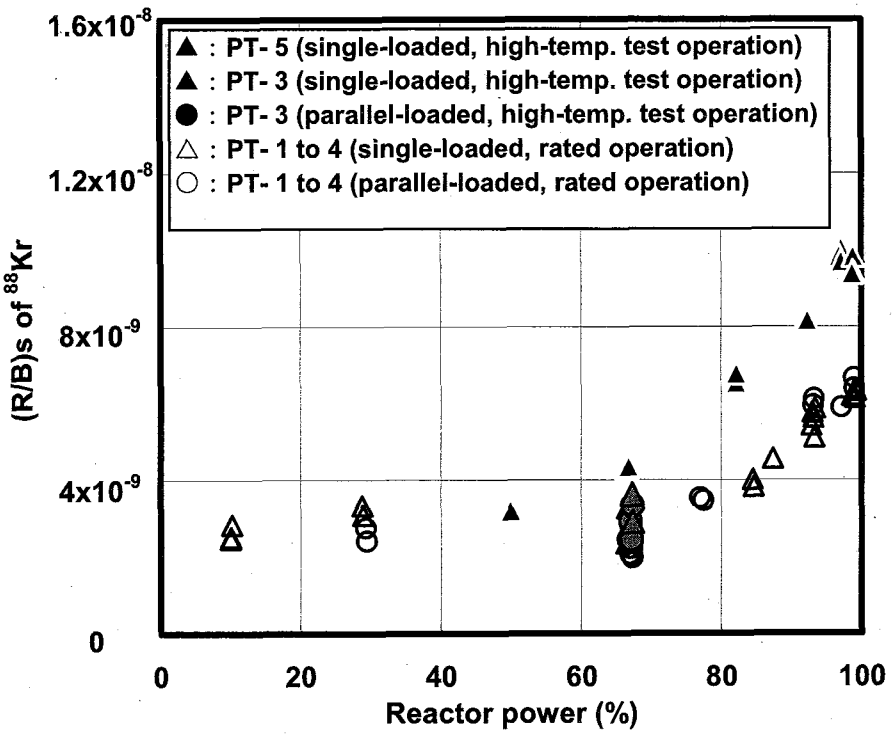

Fig. 3.7 The relationship between R/B rates of ^{88}Kr and reactor power

3.1.5 Fuel temperature evaluation[5)]

The integrity of CFPs depends on the fuel temperature strongly. It is important to evaluate the maximum fuel temperature during operation. The maximum fuel temperature needs to be estimated with numerical calculation because the fuel temperature cannot be measured directory in HTTR.

So the maximum fuel temperature at the reactor power of 30MW in high temperature test operation mode was estimated with operation data, and it was confirmed that the estimated maximum fuel temperature is lower than the thermal limit temperature of 1495°C.

(1) The comparison of the measured and estimated results at rise-to-power test

The flowchart of fuel temperature evaluation is shown in Fig. 3.8.

For nuclear characteristics estimation code CITATION, the estimated results were compared with γ-ray measurement results of the fuel assembly. This measurement was performed after rise-to-power test of the reactor power up to 9MW. It was confirmed that the measured and estimated axial-integrated power distribution for each column is almost the same as shown in Fig. 3.9.

The coolant temperature rise estimated by core thermal-hydraulic estimation code FLOWNET was compared with the measured one at the reactor power of 30MW. The comparison results are shown in Fig 3.10. The coolant temperature rise was obtained by the difference of the core inlet coolant temperature and the hot plenum coolant temperature. The difference between estimated result and measured results were less than 2%, so it was confirmed that the estimated results are almost the same as the measured results.

These facts show that the coolant flow distribution and the axial power distribution integrated in each channel are estimated correctly by FLOWNET and CITATION. These codes and the fuel temperature estimation code TEMDIM were used to obtain the reactor installation permit of HTTR for the purpose of evaluating the maximum fuel temperature.

(2) The estimated results for high-temperature test operation

The fuel temperature was estimated based on measurement data obtained in rise-to-power tests.

Table 3.3 shows the revision of fuel temperature estimation conditions. These conditions were revised from design conditions with operation data. The upper plenum temperature, primary coolant flow rate, CR positions, reactor thermal power and systematic factors were revised. Moreover, fuel burn-up day was set to 160 days of realistic high temperature test operation time.

As the result, the maximum fuel temperature on high temperature test operation was estimated as 1463°C, and it was confirmed that the maximum fuel temperature should be lower than the thermal limit temperature of 1495°C. At the reactor installation permit of HTTR, the maximum fuel temperature was estimated as 1492°C.

Table 3.3 The revised fuel temperature estimation conditions

	Information obtained from operation
Upper plenum temperature Design : 415°C Present : 409°C	Upper plenum coolant temperatures of 399°C ~ 409°C were obtained by measurement at reactor power of 30MW. So, the core inlet coolant temperature was changed from 415°C to 409°C.
Primary coolant flow rate Design : 10.2kg/s Present : 10.1kg/s	It was confirmed that removed heat by the VCS is 800kW versus 600kW of design value in rated operation and reactor power of 30MW, and that radiated heat from standpipes is 70kW. So, the primary coolant flow rate was changed from 10.2kg/s to 10.1kg/s based on reactor inlet/outlet coolant temperature of 395°C/950°C.
CR position Design : 2,610mm Present : 2,900mm	It was confirmed that CR position is 2,855mm in rated operation and reactor power 30MW. This value is higher than the design value. So, the CR positions were set 2,900mm with consideration of reactor outlet coolant temperature rise of 100°C.
Reactor thermal power Design : 102.5% Present : 102.0%	It was confirmed that the measurement error of reactor thermal power is lower than 1.5% based on the proofreading data of measurement instrument. So, the systematic factor on reactor power was changed from 2.5% to 2.0% with the consideration of control error of 0.5%.
Systematic factor of axial power distribution Design : 4.0% Present : Delete	In reactor design, fuel rods are modeled as continuous object to the fuel block end, so spike effect due to the graphite at the fuel rod end was considered as an estimation error. The effect was considered as the systematic factor of 4.0%. On the other hand, spike effect was not observed in the measurement result of power distribution. So, the systematic factor on axial power distribution of 4.0% was eliminated.
Systematic factor of flow distribution Design : Coolant temp. 4.0% Film temp. 3.2% Present : Coolant temp. 2.0% Film temp. 1.6%	In the reactor design, the coolant temperature rising factor of 4.0% and the film temperature rising factor of 3.2% were considered as hot spot factors for core effective coolant flow rate. However, it was found that estimated results of core effective flow rate were 2% more conservative than realistic core effective flow rate by comparison of measurement and estimation results. So, the coolant temperature rising factor and film temperature rising factors were set 2.0% and 1.6%, respectively.

Systematic factor of coolant temperature rise Design : 2.5% Present : Delete	In the reactor design, the effect of the thermal power proofreading error was considered as both temperature rising factor and coolant temperature rising factor for the purpose of conservative estimation. In realistic operation, the thermal power proofreading error dose not affect the coolant temperature rise. So this factor can be eliminated. (The effect of reactor inlet/outlet temperature measurement error is considered as the systematic factor of coolant flow rate separately.) So the coolant temperature rising factor of systematic factor on reactor power was eliminated.

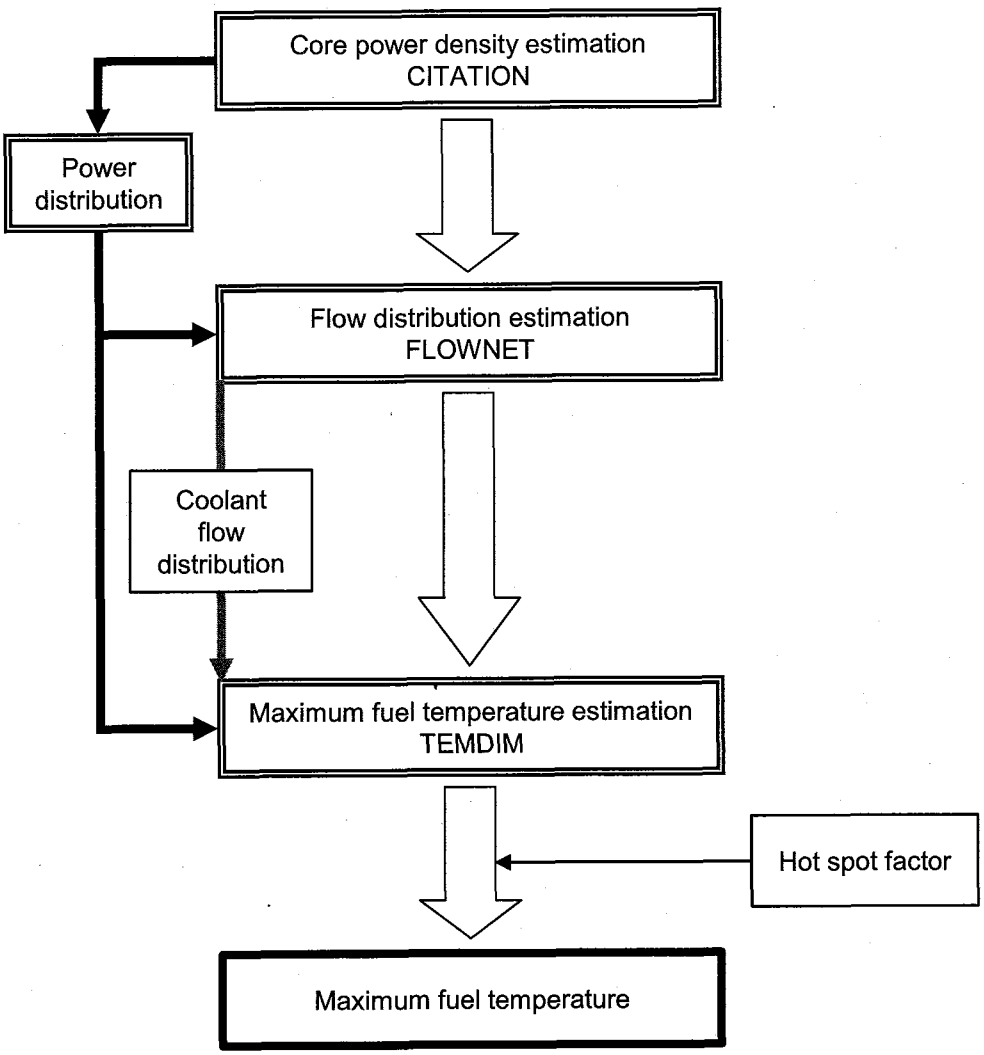

Fig. 3.8 The flowchart of fuel temperature estimation

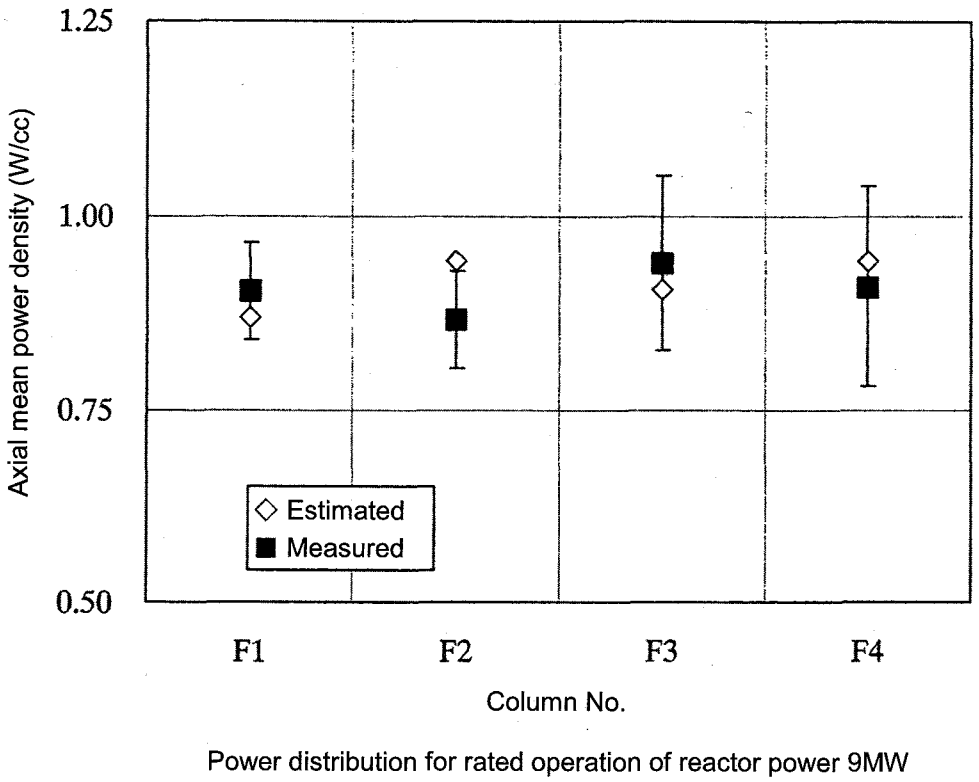

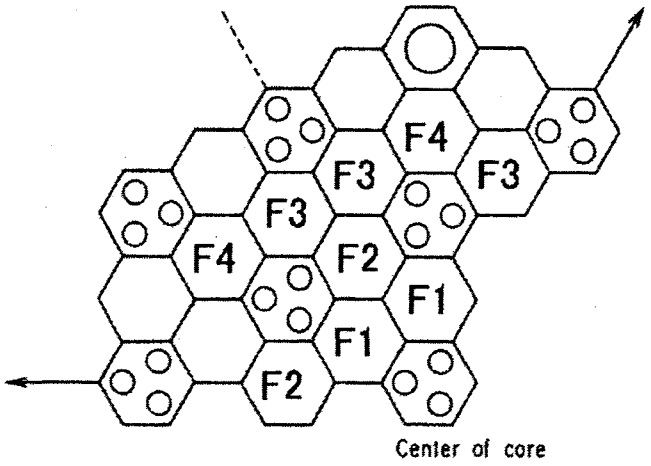

Fig. 3.9 The comparison of the estimated power distribution and the measured one

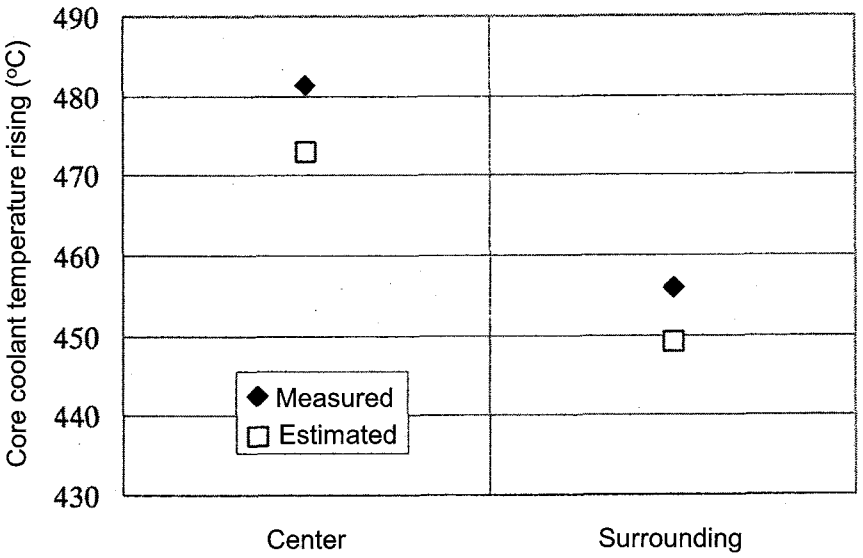

Estimated result for rated operation of reactor power 30MW
(Comparison of hot plenum coolant temperature)

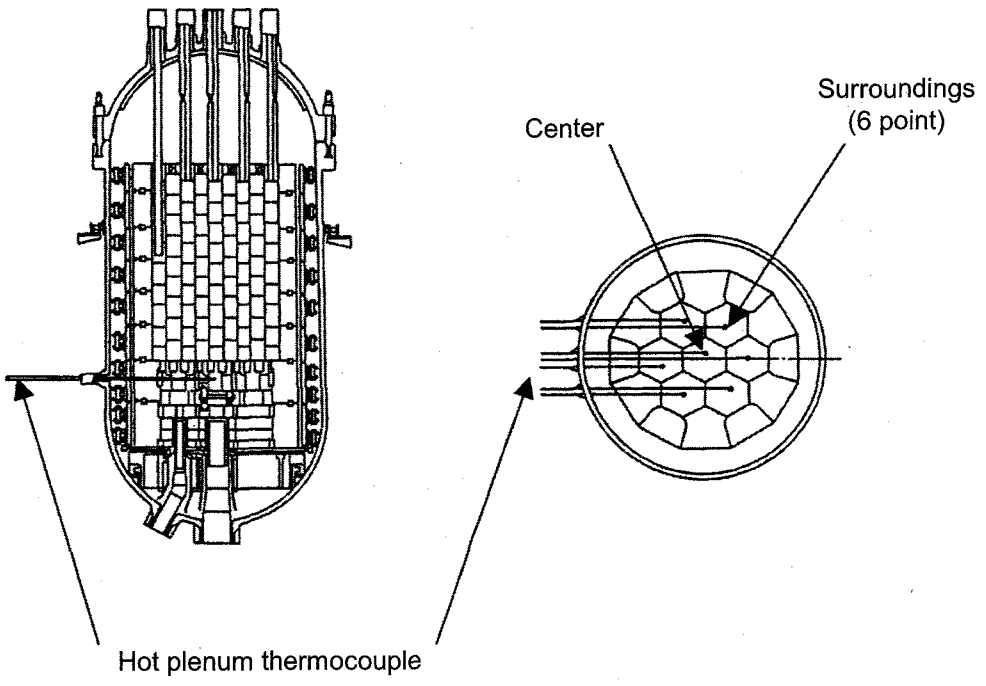

Fig. 3.10 The comparison of the estimated coolant temperature rising and the measured one

3.2 Operating experiences for the improvement of the performance

3.2.1 Filter exchange of primary gas circulators[7)]

Four Primary Helium Gas Circulators (PGCs) are arranged in the primary helium circuit, three are arranged around the PPWC and the rest is arranged around the IHX as shown in Fig. 3.11. The PGC is a centrifugal, dynamic gas bearing type. Figure 3.12 shows a bird's-eye view of the gas circulator. The gas circulator consists of the following components: the electric stator and rotor assembly, the internal structure, the bearing, the impeller and the filter.

The filter unit, which is on the top of the circulator, protects the impeller and rotating shaft from dust, and it is made of sintered metal SUS316. Figure 3.13 shows the differential pressure rise at the filters around the PPWC. It was observed from 1999 and reached 26.4kPa. This value corresponds to 33.7kPa for rated power, which is over the alarm level of 30kPa.

Therefore, the filters of PGCs were exchanged after the 1st operation cycle (RS-1). The filter exchange carried out at the period of periodic inspection in 2002.

Before the work, planned exposure, exchange procedure, etc were investigated with the mock up test, that simulated the actual filter exchange. Main exchange work steps were as follows:

① Assemble greenhouse
② Remove the top plate of the gas circulator
③ Auxiliary shielding and temporary storage tank installation
④ Bring the filter into the storage tank
⑤ Movement of the storage tank
⑥ Installation of the new filter
⑦ Installation of the top plate of the gas circulator
⑧ Dismantling greenhouse.

The picked-up filter surface was observed in order to investigate the cause of differential pressure rise. Figures 3.14 and 3.15 show the filter surface. The foreign adhesion material was the thermal insulator and the carbon as shown in Fig. 3.16. This foreign material was monitored to identify cobalt-60 (^{60}Co) and Antimon (^{124}Sb) that were corrosion products. The evaluated personal exposure was about 0.42mSv less than the planned exposure about 1.8mSv.

The filter exchange was completed successfully without any contamination.

The differential pressure after the filter exchange was measured as 2.5kPa at full-power of 30MW, which was much lower than the predicted one.

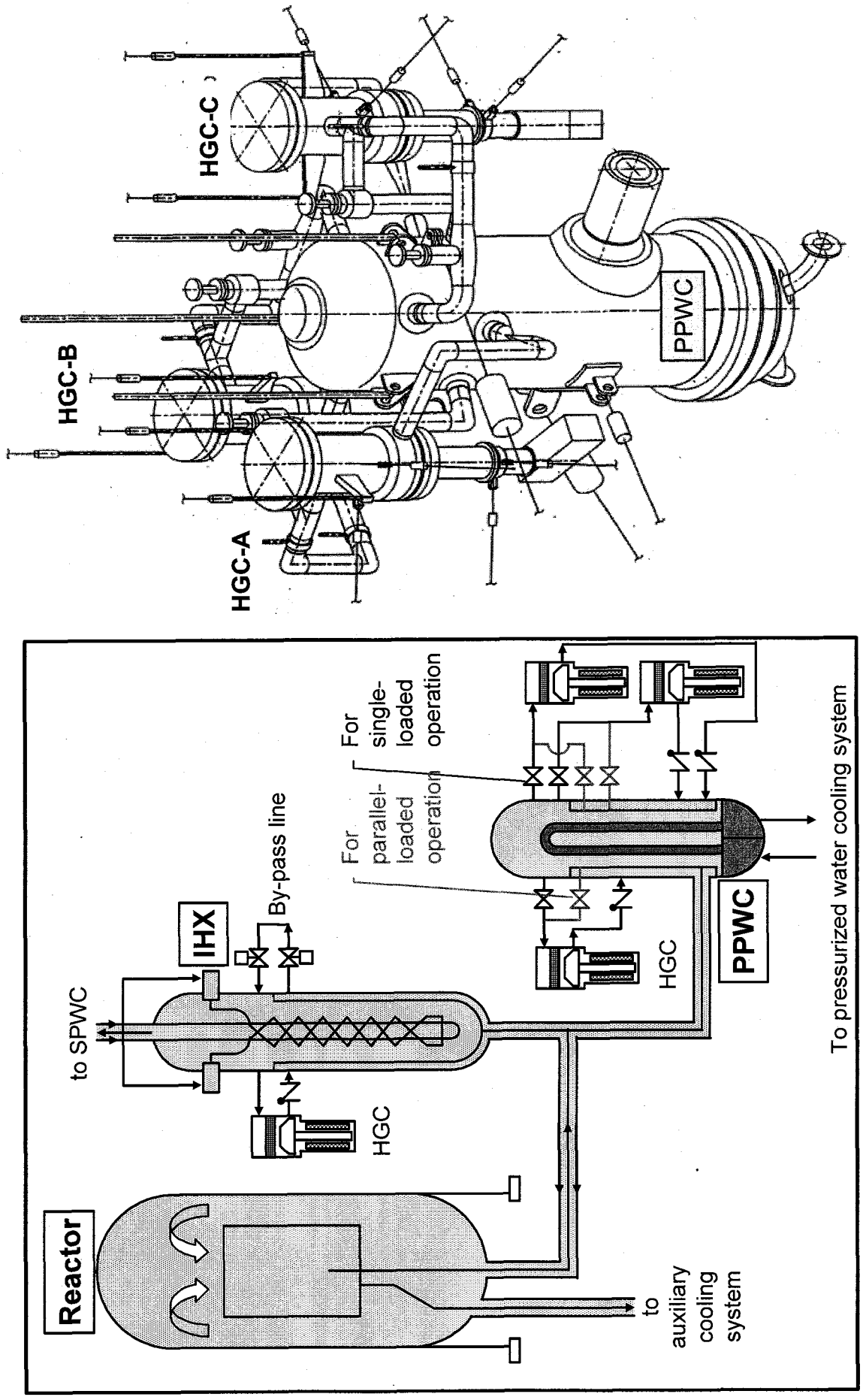

Fig. 3.11 The arrangement of primary helium gas circulator

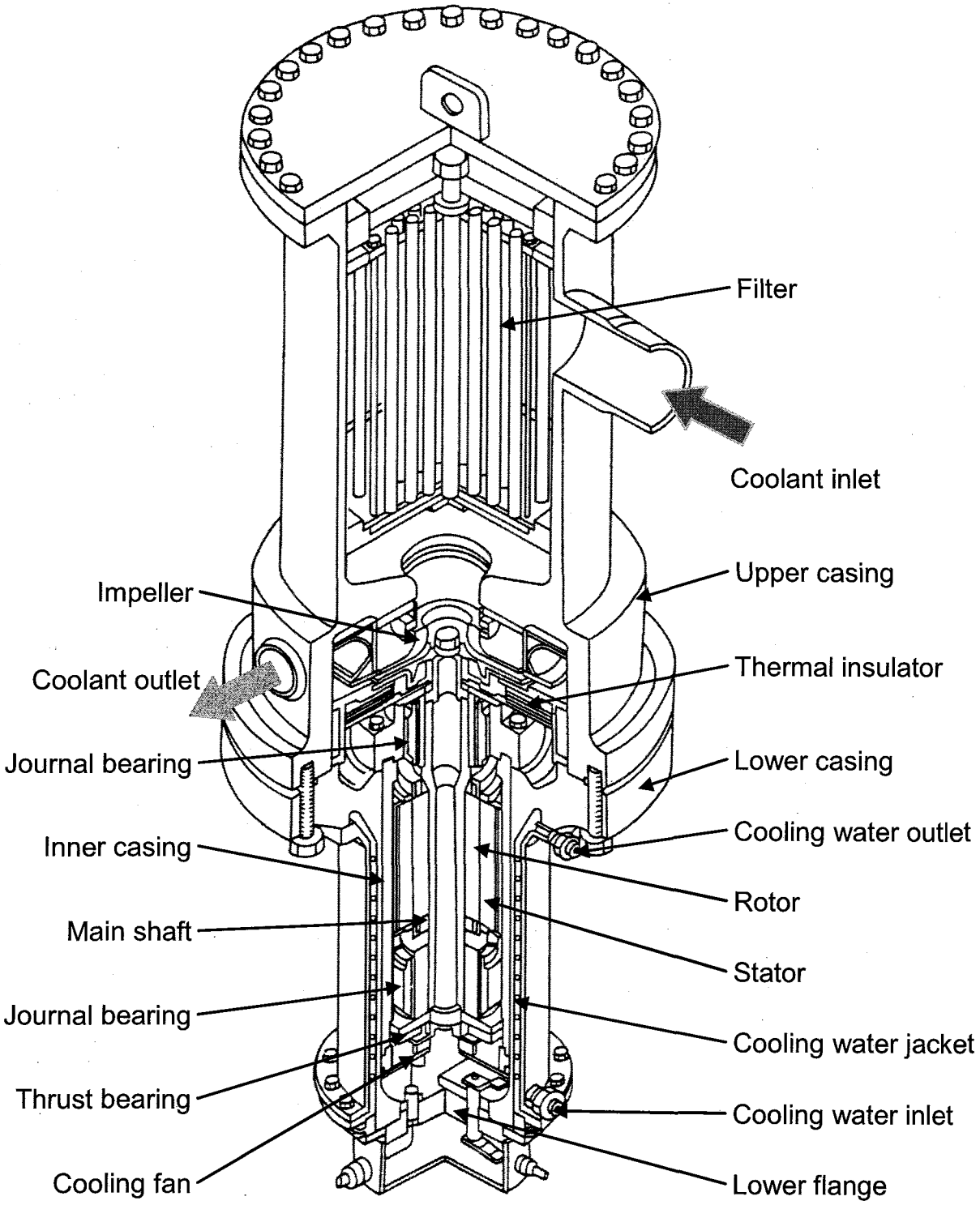

Fig. 3.12 The structural diagram of helium gas circulator

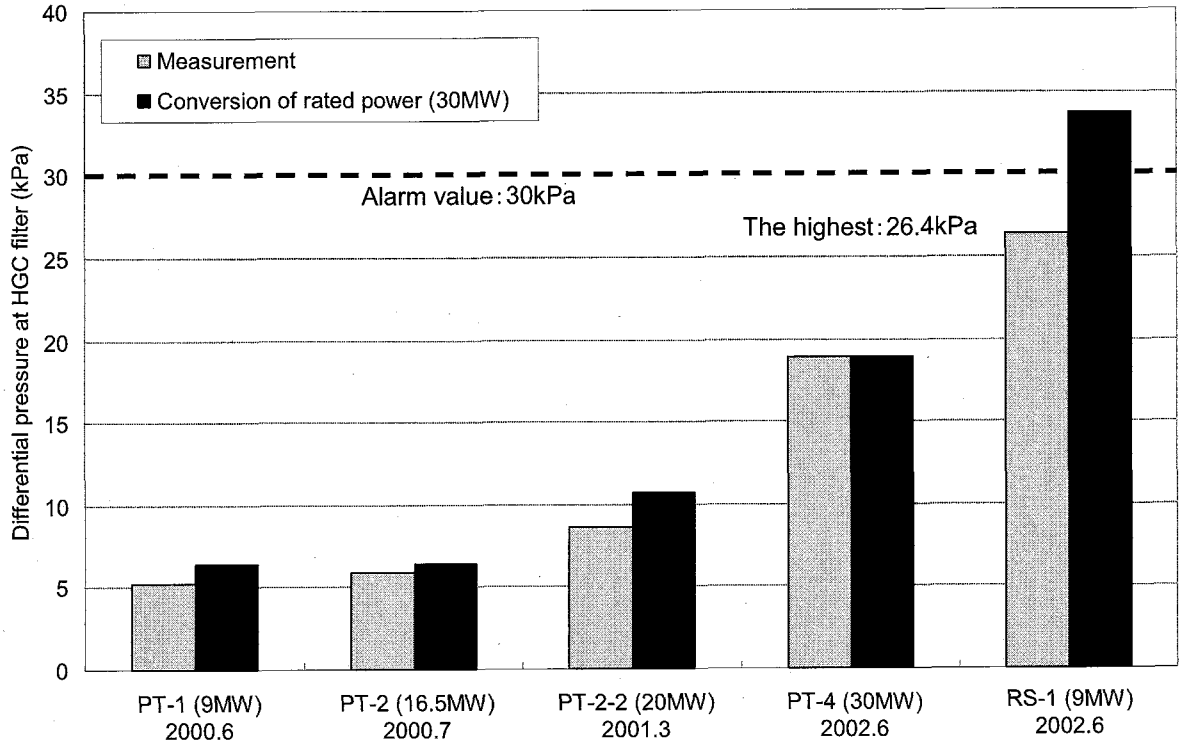

Fig. 3.13 Increase of differential pressure of the PGC filter

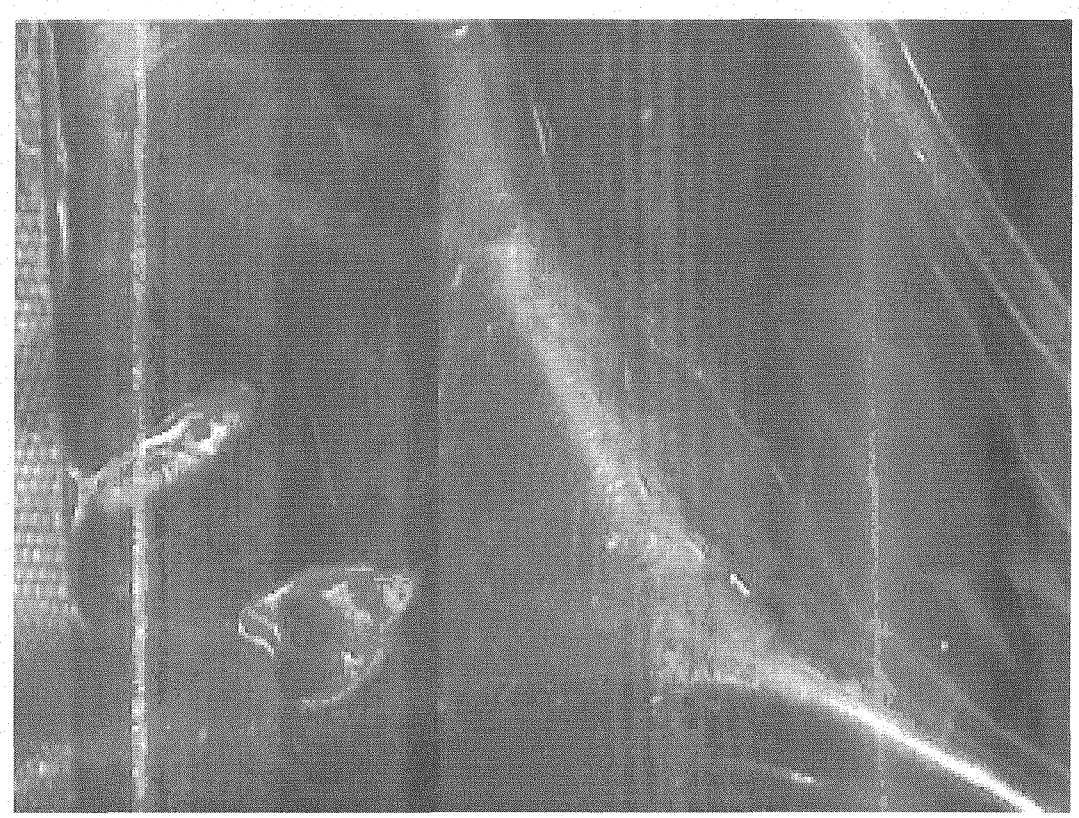

Fig. 3.14 The photograph of the filter surface (1)

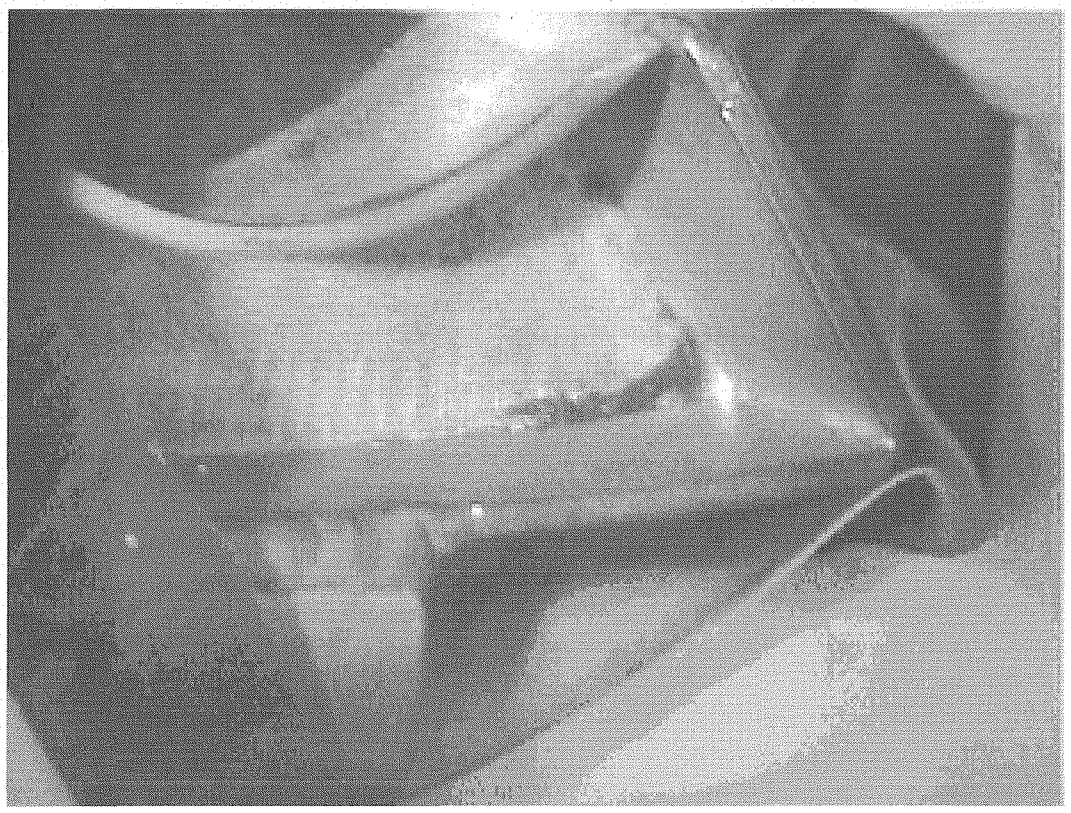

Fig. 3.15 The photograph of the filter surface (2)

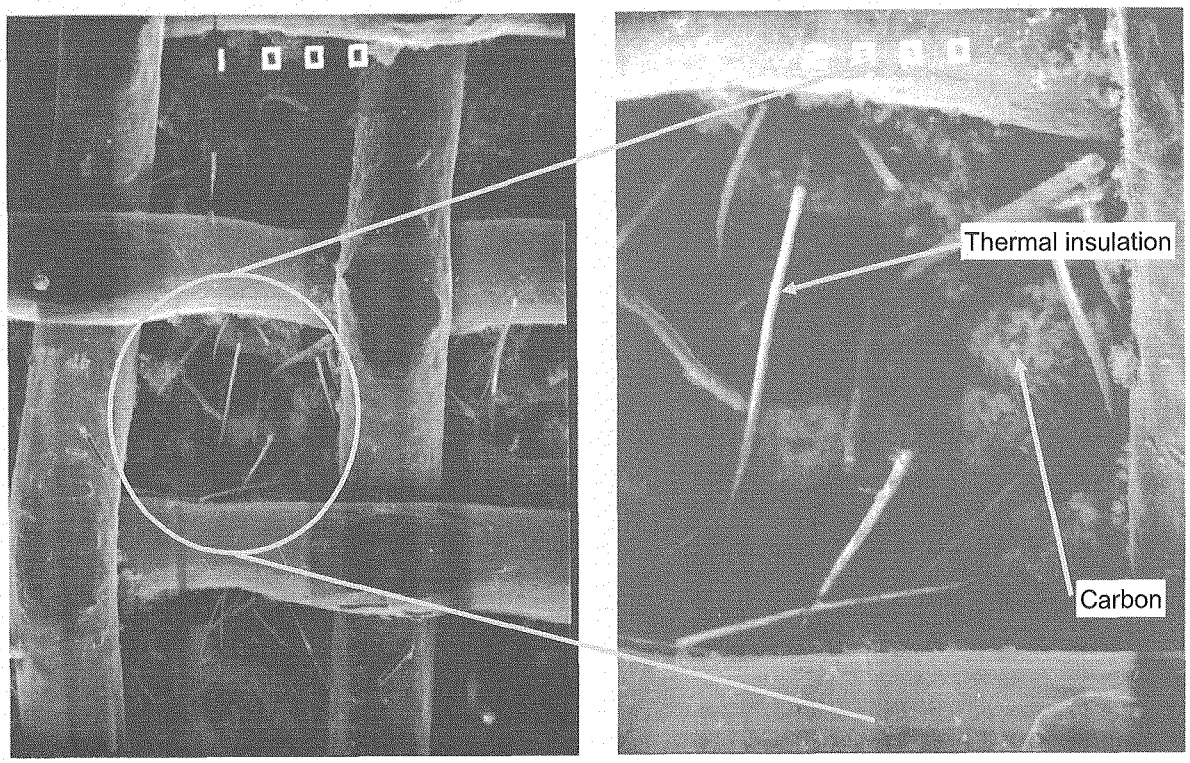

Fig. 3.16 The SEM image of the PGC filter surface

3.2.2 Installation of the windshield panels to improve air-cooler performance

The pressurized water cooling system is installed to cool primary coolant and secondary helium coolant at the PPWC and the SPWC. This system consists of a pressurized water pump, an air-cooler and so on. The heat, which is conducted through the PPWC and the SPWC, is finally transferred to the atmosphere by the air-cooler. The air-cooler consists of heat transfer tubes with fins, 6 fans and so on. The heat removal capacity is 30MW at 2600t/h airflow rate. The air-cooler is set up at the middle stage of reactor building as shown in Fig. 3.17.

At 3rd phase rise-to-power test, the heat removal capacity of the air-cooler decreased due to change of the wind direction. Therefore, the cooled water temperature was rose for a few hours and reached steady state. Typical response of the cooled water temperature is shown in Fig. 3.18. By the analysis, it was shown that the heat removal capacity of the air-cooler decreased by the East-North-East (ENE) and North-East (NE) wind. Figure 3.19 shows the numerical simulation results of air behavior around the air-cooler. It was shown that the phenomena were caused by the re-entry of the discharged hot air into the inlet of the air-cooler.

It was expected that the installation of the windshield panels between the air cooler and the reactor building should improve the heat removal capacity. The overview of the windshield panels is shown in Fig. 3.20. As the results of analysis, the inhalation-discharge ratio of air at the air-cooler has been less than 5% by the installation of the windshield panels at North, East and South.

This improvement useful for the heat removal capacity of the air-cooler, and the increasing of air-inlet temperature has not appeared.

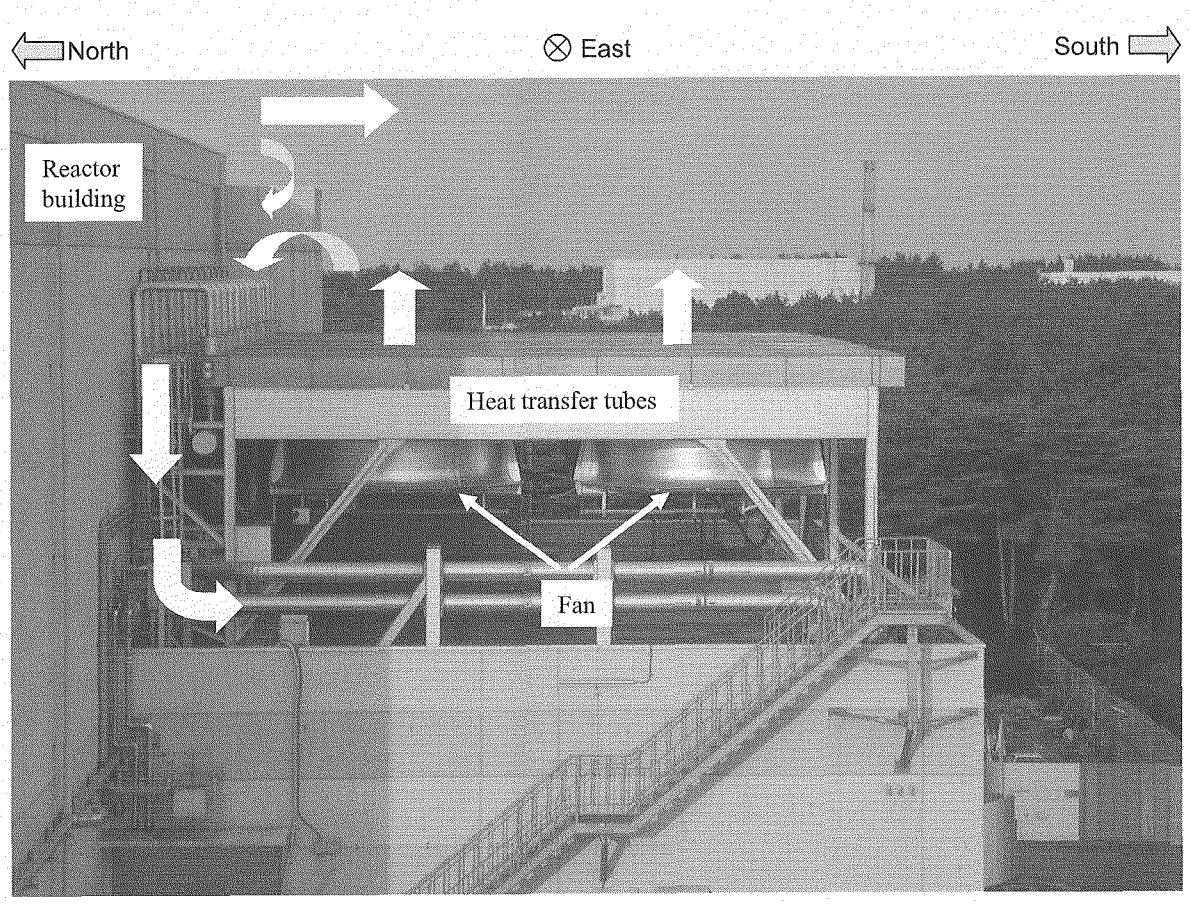

Fig. 3.17 The overall view of the air-cooler

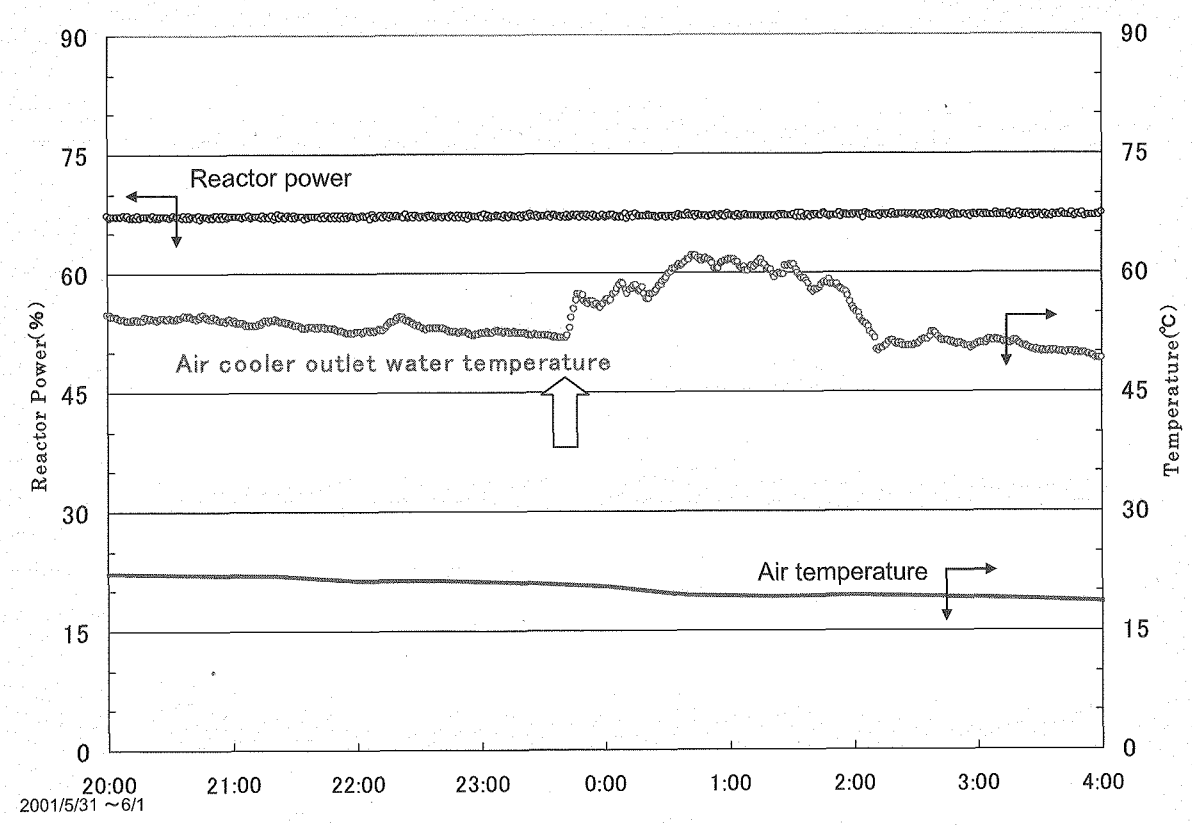

Fig. 3.18 The time variation of the air-cooler inlet air temperature and the air temperature

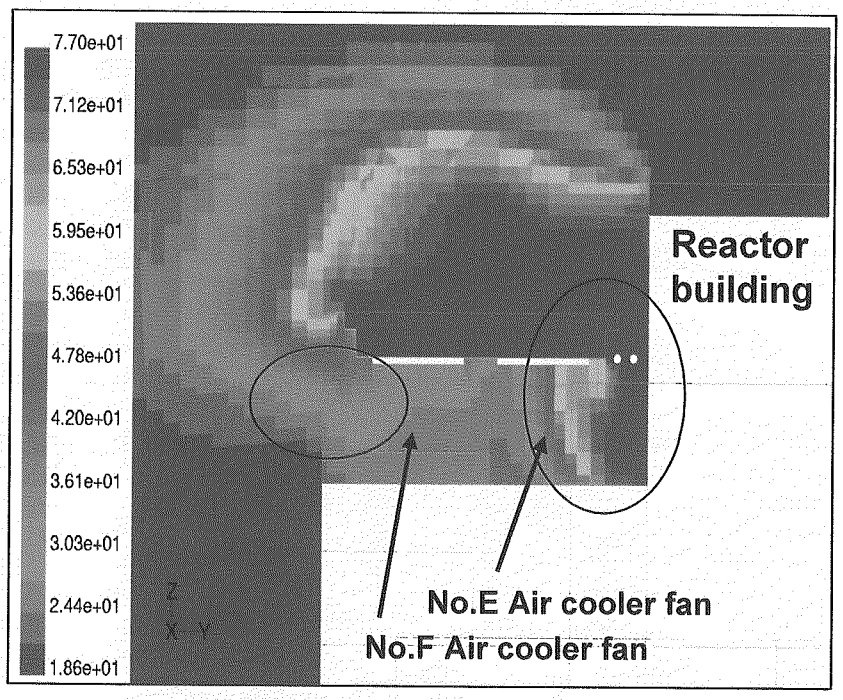

Before improvement

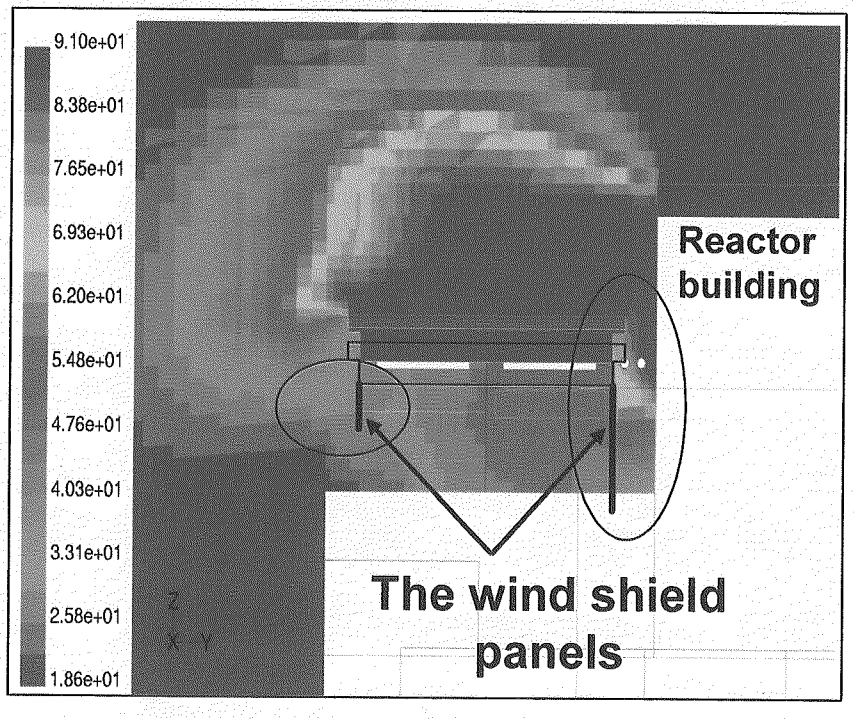

After improvement

Fig. 3.19 The effect of the wind shield panels (calculation, 3-D)

This is a blank page.

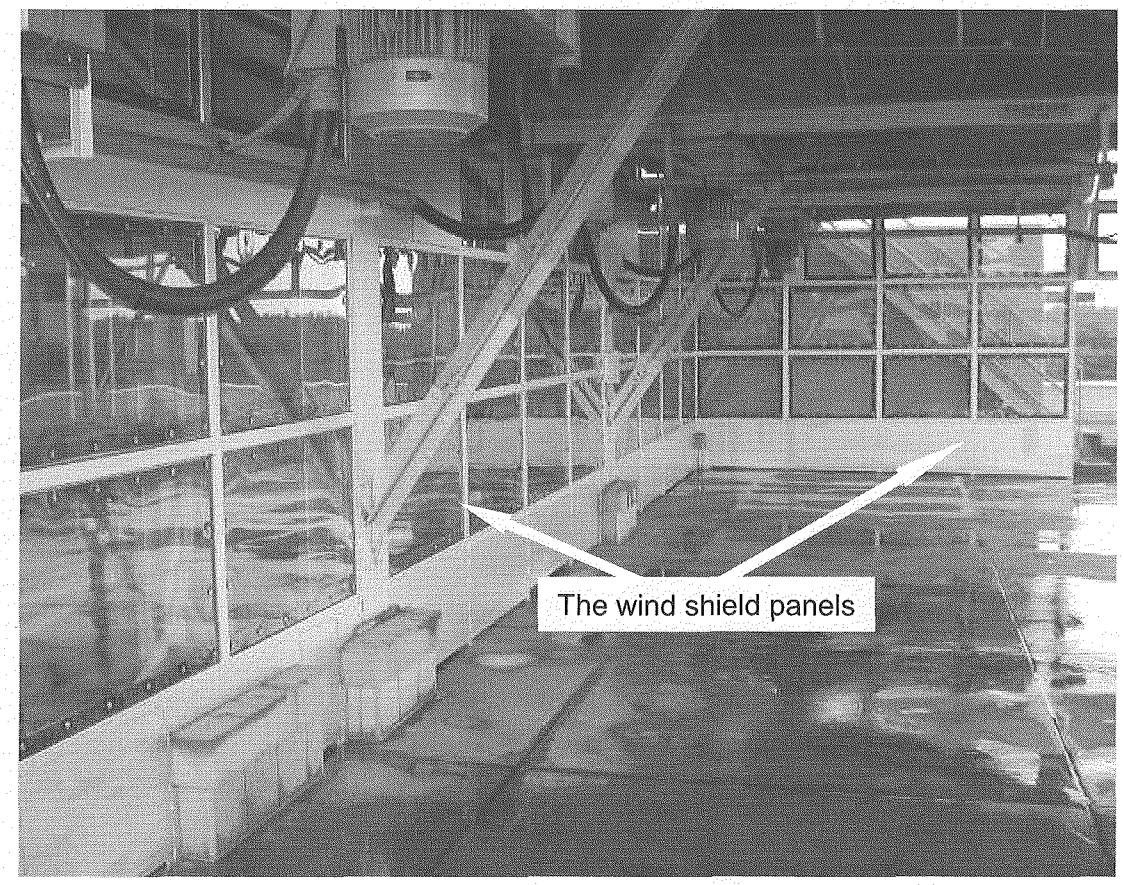

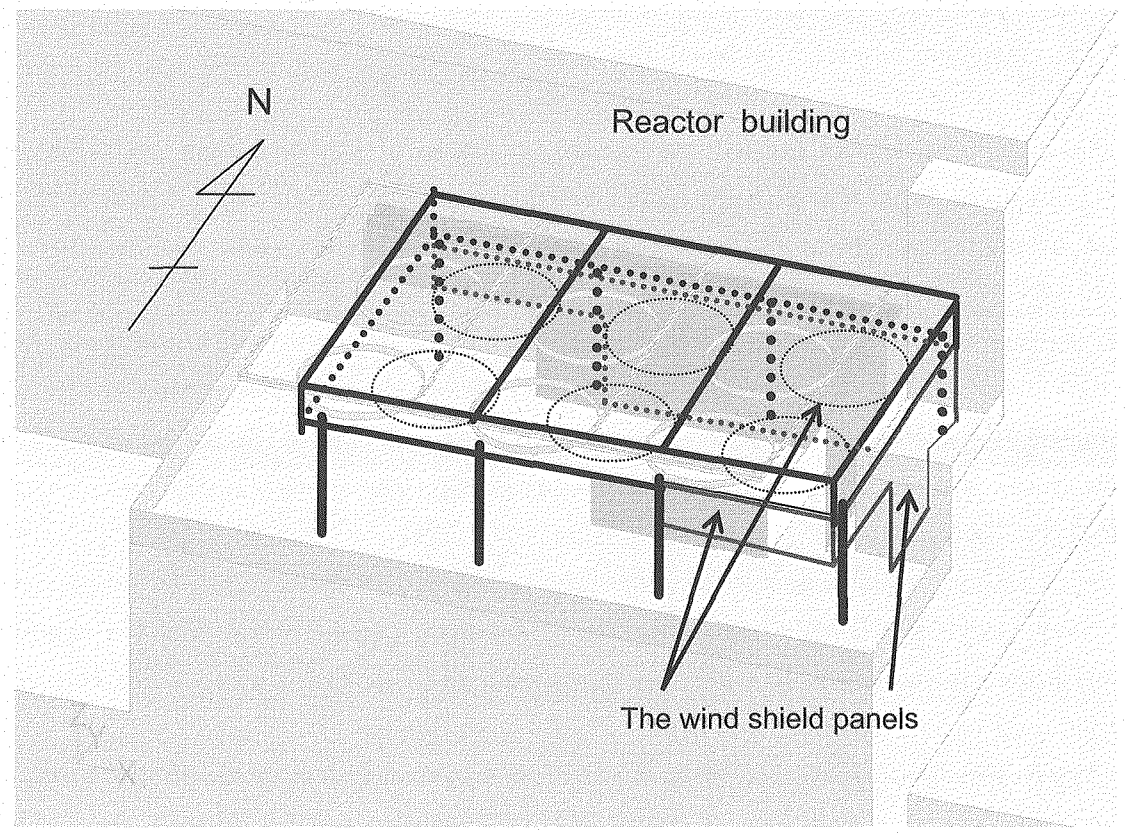

Fig. 3.20 The installation of the wind shielding board

3.2.3 Inferior of the Reserved Shutdown System (RSS) actuation[8)]

The 3rd periodic inspection of HTTR had progressed from Jul. 26, 2004 to Mar. 4, 2005. During the RSS movement inspection before reactor start-up, it was found that the position lamp of the R1-3 RSS, one of the 16 pairs RSS, did not actuate on Feb. 21, 2005. However, the RSS actuated with smoothly on Feb. 27, 2005. By the comparison between R1-4 RSS (normal) and R1-3 RSS (abnormal), the causes were expected that a brake of the driving motor of the RSS had some trouble. The overview of the RSS is shown in Fig. 3.21.

The following investigations were carried out and obtained results after decomposition of the R1-3 RSS were as follows:

- Inspection of the control panel and the control machine was carried out. There was no problem such as cable insulation level and voltage level and so on.
- Some wrong parts were discovered such as a distortion of the oil seal at the driving motor shown in Fig. 3.22. It was found that a mixture had adhered to the brake part. The mixture was made of the sealing-oil and the defacement powder produced by abrasion of the brake.
- There was no failure at any other parts.

It was cleared that both the distortion of oil seal and the mixture adhered to the brake part caused an inferior actuation of the RSS.

The cause was investigated as follows:

1) The investigation was carried out except the cause of the distortion. The obtained results showed that there was no fact of overheating because sufficient lubrication oil was inside, the width of frictional wear was smaller than the factory result and dimensions of the oil seal satisfied the design.
2) To confirm the adhesion of the brake parts and to investigate the behavior of the mixture, the simulation test was carried out. As the results, it had cleared that the mixture showed the maximum adhering force at mixing ratio of 25wt% (the sealing-oil: 75wt%, the brake powder: 25wt%), and it was confirmed that the same phenomena as those on Feb. 21, 2005 reappear.

Therefore, it was concluded that the distortion of the oil-seal occurred at the beginning of fabrication process in the factory. So, the intruded oil and brake powder mixed, and the kneaded mixture caused the phenomena.

The confirmation test was carried out in order to detect the oil intrusion into break. It was confirmed that electric current changing time of the brake with oil intrusion is larger than that without oil intrusion, and the continuous time of the motor start-up electric current with oil intrusion is larger than that without oil intrusion.

The causes why the R1-3 RSS was not actuated was 1) the distortion of an oil seal that occurred at the beginning of fabrication process in the factory, and 2) the adhesion of brake by sufficiently kneaded mixture made of sealing-oil and defacement powder.

By the confirmation test, it can be adopted the above detection method that was measurement of electric current changing time of the brake and continuous time of the motor start-up electric current.

It was confirmed that the other RSSs were actuated without oil intrusion by measuring both of the change time with break electric current and continuous time of motor start-up electric current.

Corrective actions were taken as follows:

(1) The motor of the R1-3 RSS was replaced with the new one.

(2) It was decided to perform the RSS actuation inspection monthly, which include measurement of both of the brake current changing time and the continuous time of the motor start-up current.

(3) All of the motors used in the RSS shall be changed within 5 years

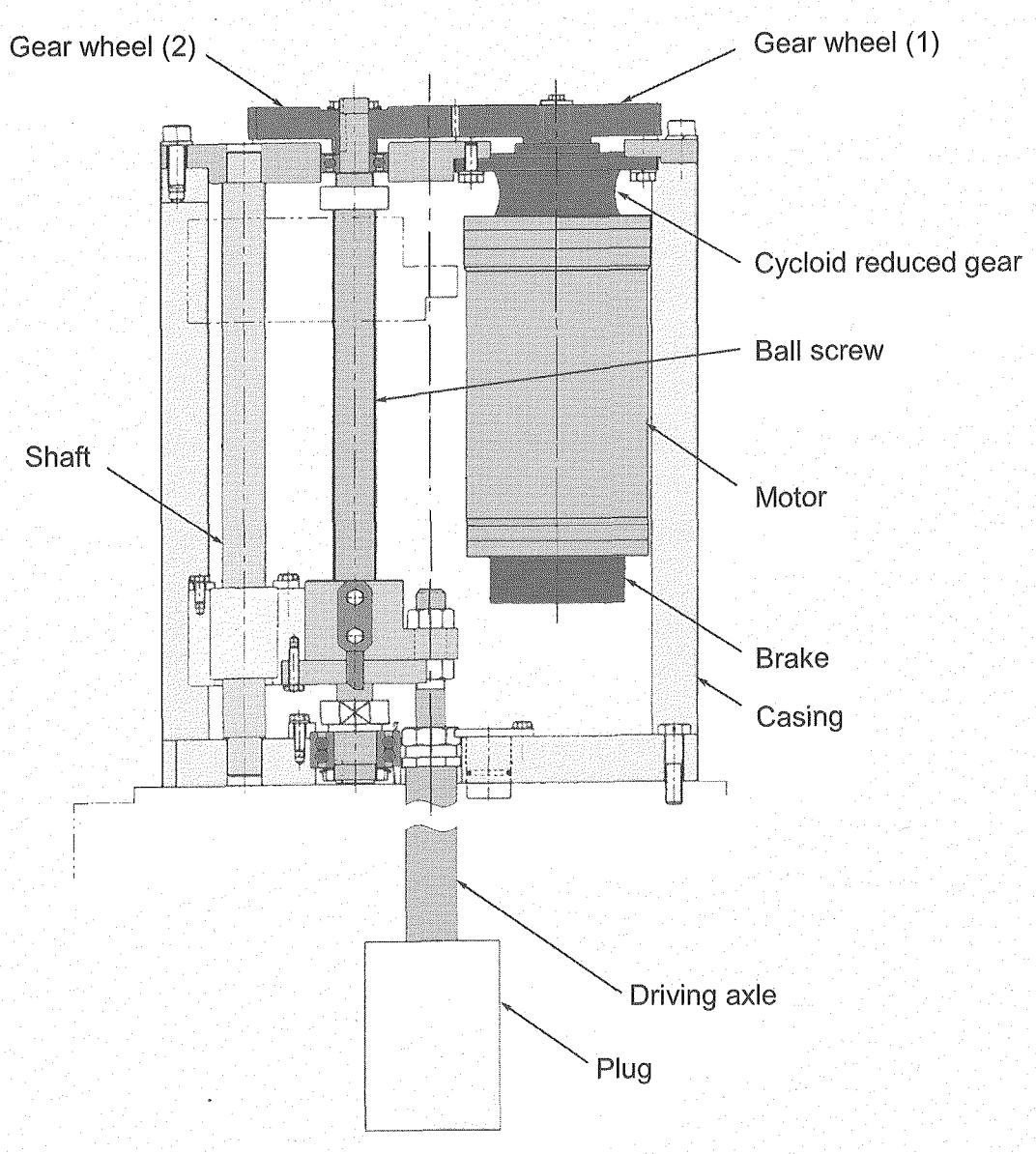

Fig. 3.21 Schematic diagram of the RSS driving unit

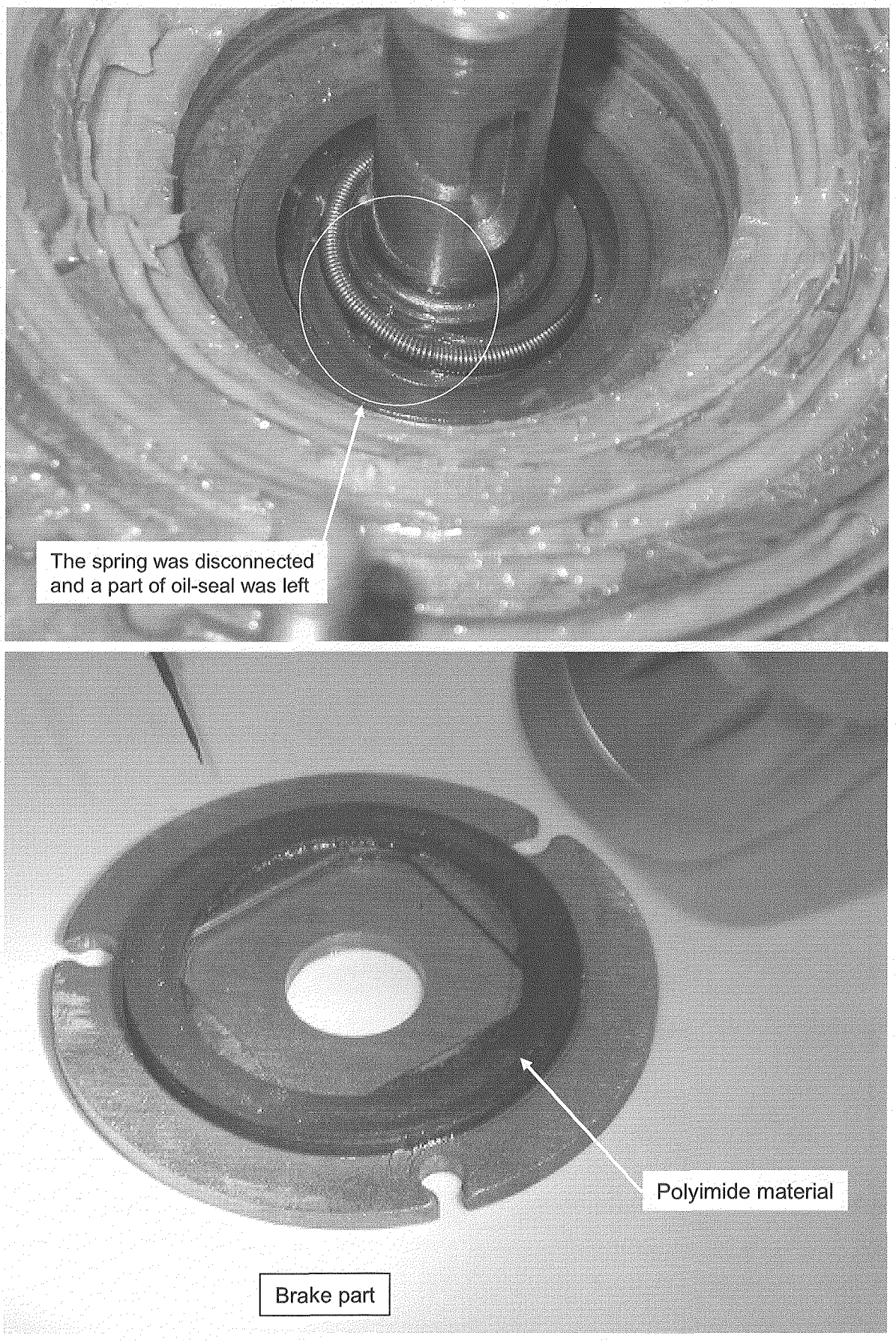

Fig. 3.22 The oil seal at motor of the R1-3 RSS

3.2.4 Contact failure of signal lead wire in WRM

The three developed neutron sensor for the wide range monitoring system (WRM) are installed inside the reactor pressure vessel of HTTR. The WRM environment temperature is 450°C under normal operation and 550°C under an accident. The specification of the WRM is shown in Table3.4. The WRM is designed to satisfy the requirement for the safety protection against the accident during start-up and for post-accident monitor.

The design features of the WRM shown in Fig.3.23 are as follows:

- The gas used in the first chamber at high-temperature environment was studied in order to obtain large output pulse and short collection time performances with low voltage in the pulse operation mode. A Argon-Nitrogen-mixed gas was chose for the purpose of the achievement of the aim.
- A double chamber structure is applied. The inner chamber is provided separately and insulated from the outer chamber and is connected to the inner sheath of the triple axial MI cable with high quality. The most important reason why the double chamber structure is employed is to protect the metal ceramic seals from higher-pressure and high-temperature.
- The fission material (enriched Uranium-235 (^{235}U)) is coated on both of the electrodes for manufacturing a small chamber.

On Sep. 14, 2005, the count rate of Channel-I showed zero which continued for 2 days. After that, the count rate showed 20cps. During the 2 days, it cleared that :

1) Pulse signal from the chamber was not observed.
2) Measured capacitance showed a small deviation compared to that in an periodic inspection.

The measured deviation was the capacitance between the signal lead wire and MI-cable. The other channels of Channel-II and Channel-III showed the normal pulse signal and normal capacitance. The count rate of Channel-I recovered to the level of other WRMs. The historical trend of the Channel-I is shown in Fig. 3.24.

The contact failure of the signal lead wire in the WRM was investigated as follows:

(1) Investigation of the operation record

Operation data such as flow rate, vibration, reactor power, and operation time as well as radiation dose since manufacture were investigated and no abnormal data was found. These data at used condition were less severe than the confirmed test conditions of the research and development.

(2) Inspection of the fabricated data

Comparing the channel-I with the others, an abnormality such as capacitance,

resistance, pulse high and sensitivity were not observed.

(3) Investigation of cause

The integrity of lead wire/MI-cable and an inner chamber/signal lead wire were investigated. It was fairly confirmed by the experiment and check that those points were the weakest point.

The cause was cleared as follow:

The lead wire/MI-cable and an inner chamber/signal lead wire were welded by a DC welding method. The lead wire was melted and the diameter of the lead wire had become small because the welding time of this method was long. Using pulse-welded method, the welded time was short and the diameter was not changed. The comparison of strength between a DC welded and a pulse welded is shown in Table 3.5 and the both welding points are shown in Fig. 3.25.

Corrective actions were taken as follows:

The welding method was changed from a DC welding to a pulse welding. The strength of the welding signal lead was not so much changed from no-welding one.

Table 3.4 The specifications of the WRM in HTTR

Size	Outer diameter	38mm
	Overall length	352mm
Material	Outer chamber	Inconel
	Inner chamber	Inconel
	Electrodes	Inconel
	Insulator	Alumina- Ceramics
Performance	Neutron sensibility	0.12cps/nv
	Operating voltage	0～200V
	Pulse height	～1.97 μA
	Max. temperature (PAM)	550°C
	Working temperature (Normal operation)	450°C

Table 3.5 The comparison of the strength between DC welded and Pulse welded for the signal lead wire

	Strength (N)
DC welded	19.6
	34.3
	24.5
Pulse welded	45.1
	41.2
	49.0

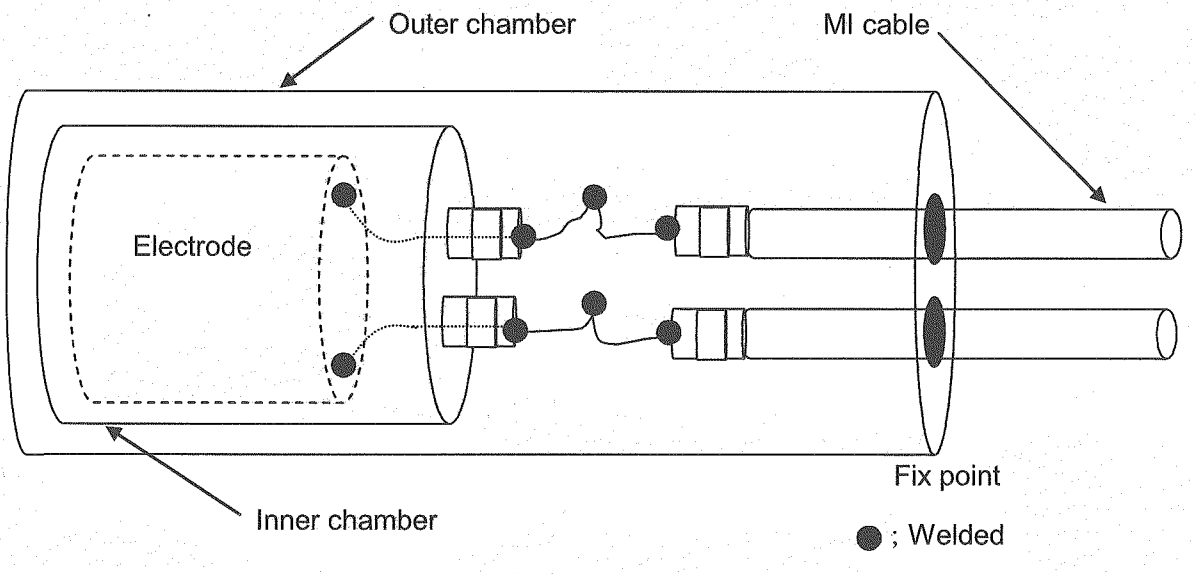

Fig. 3.23 The schematic diagram of the WRM

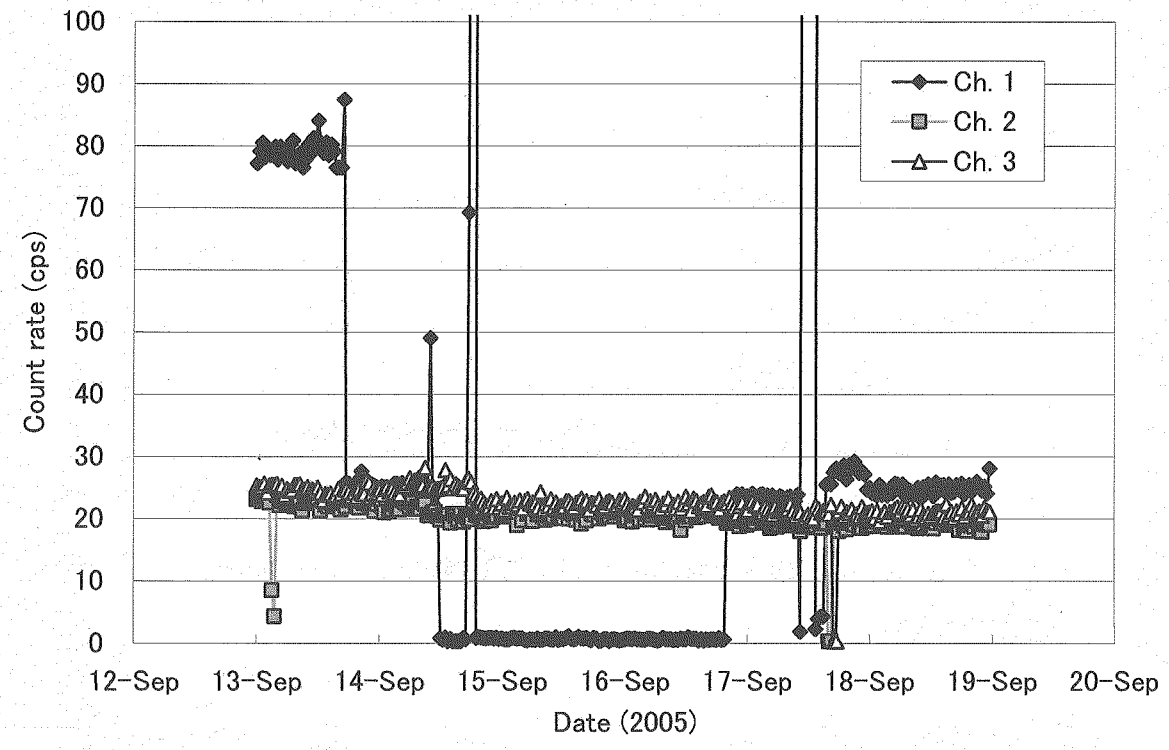

Fig.3.24 The time variation of the WRM count rate

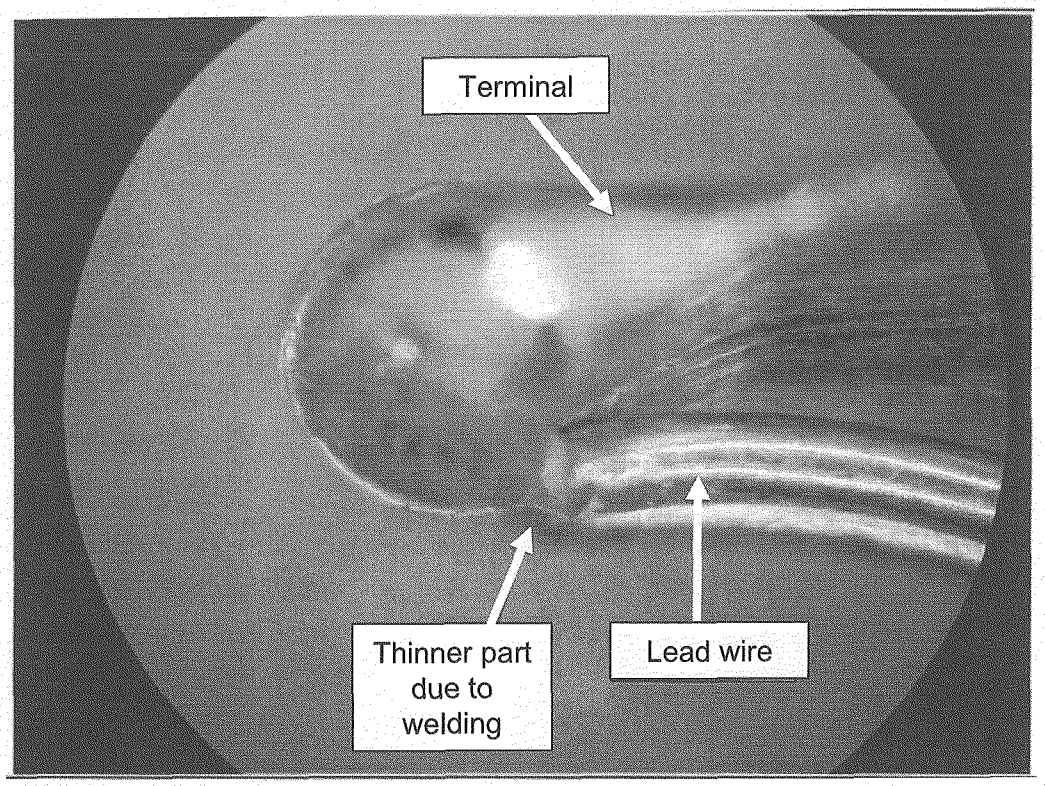

DC welded

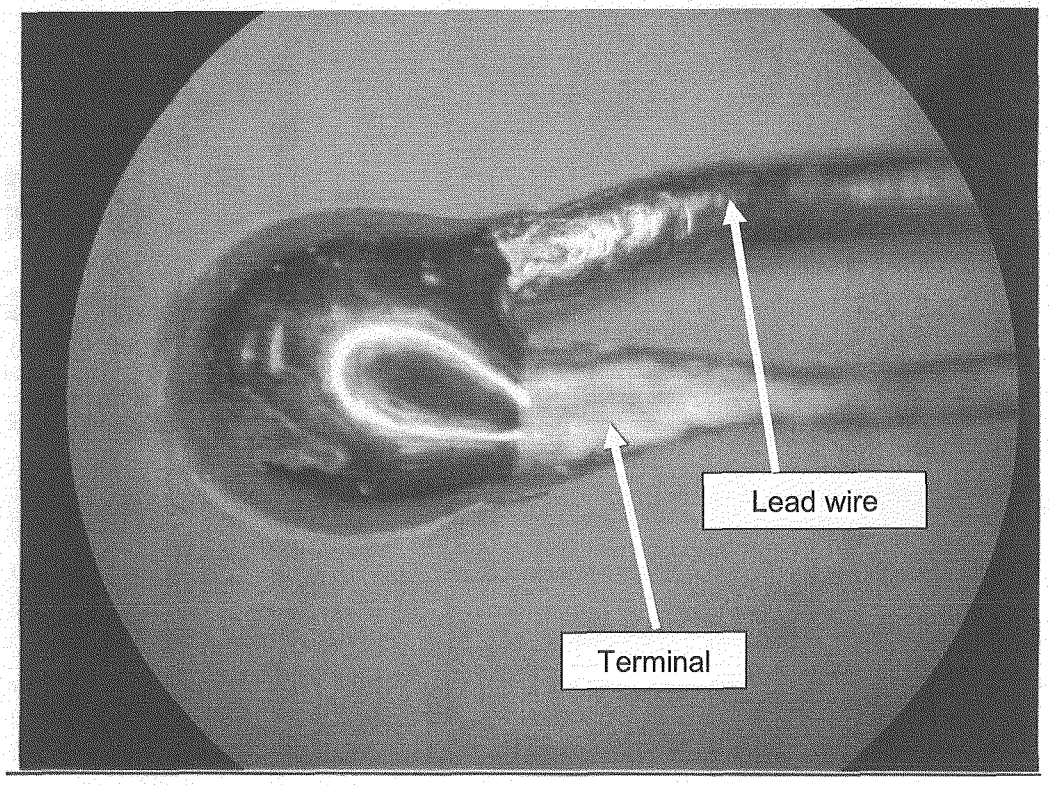

Pulse welded

Fig. 3.25 The welded lead wire

3.3 Operating experiences on failure of system and components

3.3.1 Reactor scram by pseudo-signal of vibration sensor[10)]

During power-up from 16.0MW to 16.8MW in the 2nd phase rise-to-power test on July 8, 2000, the reactor scrammed automatically by the reactor scram signal of "Primary coolant flow rate of PPWC: Low". The reactor scram signal was caused by the PGC tripping which was caused by cutoff of the power supply to the PGC (A) by the signal of "Vibration of PGC (A): High". The transient of the reactor scram is shown in Fig. 3.26. The progress of the reactor scram was as follows:

① The vibration signal from one of the PGC(A) vibration sensor reached a circulator trip level.

② PGC(A) was tripped due to cutoff of the power supply to the circulator by the signal of "Vibration of PGC (A): High" generated by the vibration signal.

③ Total primary coolant flow rate decreased by tripping of PGC(A) and reached a reactor scram level. The reactor scram signal of "Primary coolant flow rate of PPWC: Low" was initiated.

④ The reactor scram circuit breaker was opened by the scram signal.

⑤ Other PGCs of PGC(B) and PGC(C) were tripped by the scram signal.

The cause of the reactor scram was investigated as follows:

The signal had one sharp pulse for a very short time. There were four vibration sensors at a PGC. The signal of one sensor reached trip level, whereas the other sensors did not. The temperature of circulator bearings, the adjacent equipments, the sensor circuit etc. had no problem. However, there were no problems in the equipments, so the signal was predicted to be a pseudo-signal. It was supposed that the abnormal signal was observed when the sensor was heated, but the source of the pseudo-signal has not been identified.

Corrective actions were taken as follows:

Some countermeasures as shown in Fig. 3.27 were applied to prevent the pseudo-signal such as the thermal insulation between the PGC and the sensor, fixation of the MI cables. Additionally, the gas circulator trip mode was modified, so that the gas circulator trip signal become effective when the vibration signal exceed the circulator trip level and elapsed for a longer period than that before, and only when both the vibration sensors attached to upper and lower parts of the bearing casing make signals over the trip level.

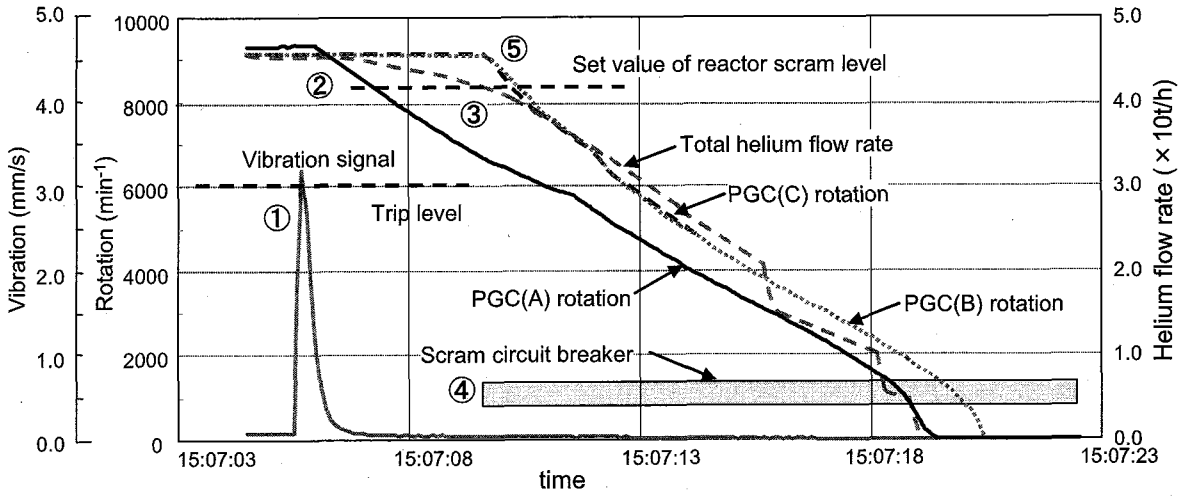

Fig. 3.26 The time transient of the reactor scram by vibration signal of PGC (A).

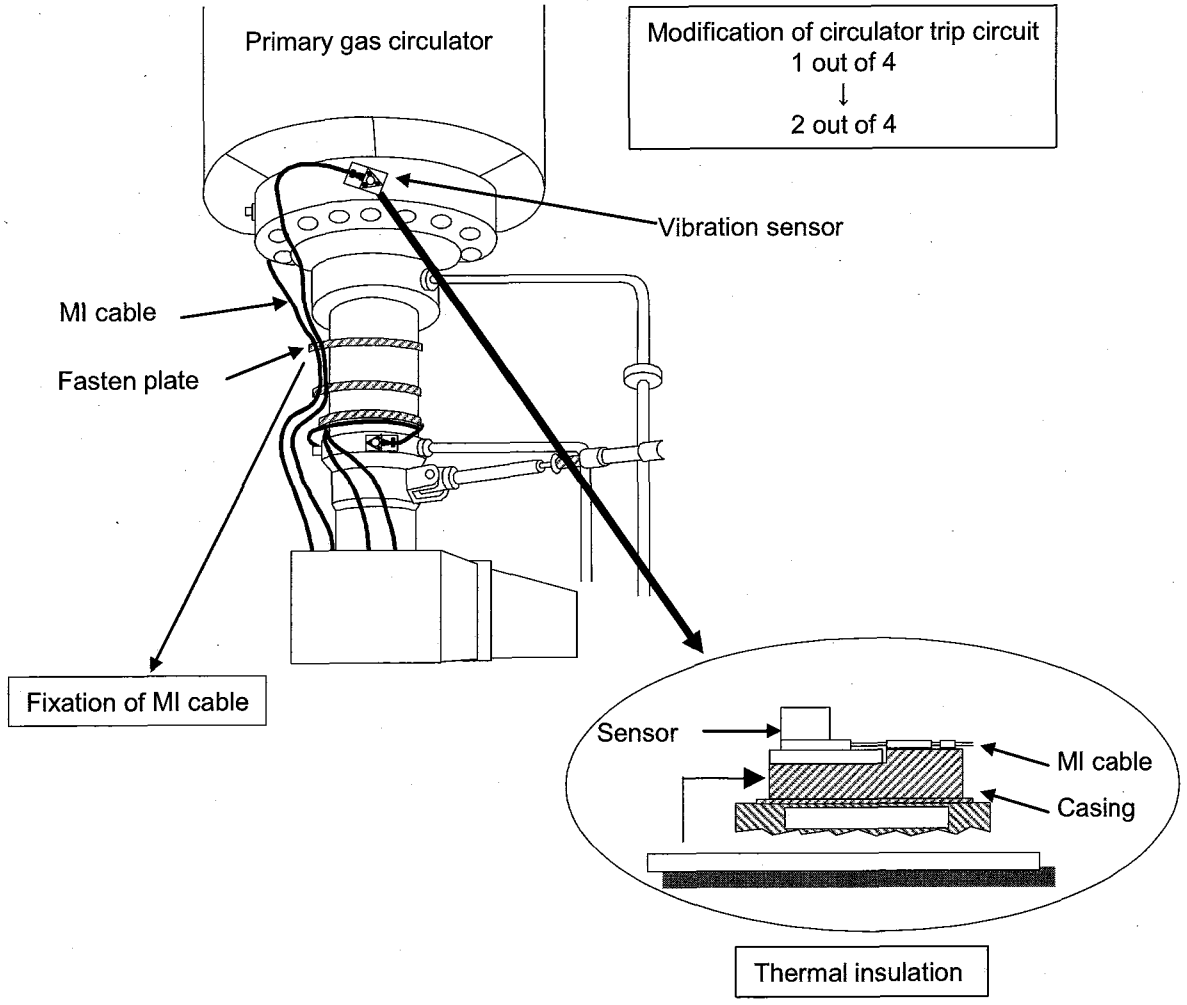

Fig. 3.27 The countermeasure to prevent the reactor scram

3.3.2 Reactor scram by malfunction of a relay for a primary gas circulator[9)]

The primary cooling system of HTTR has two heat exchangers in parallel: the IHX and the PPWC. The primary pressurized water cooler has three PGCs (A, B and C) (see **Fig. 3.28**).

During operation at thermal power of 60% (18MW) and at rated/parallel-loaded operation mode in which the two heat exchangers of the IHX and the PPWC in primary cooling system were used, the reactor scrammed automatically by the reactor scram signal of "Primary coolant flow rate of PPWC; Low" on May 21, 2003.

At first, the operation record was investigated. The helium flow rate of the PPWC decreased below the scram level of 93% of the rated flow rate (see **Fig. 3.29**) due to the PGC (A) tripping. The other two PGCs (B) and (C) coasted down by the reactor scram signal.

The cause of the trip of the PGC (A) was investigated as follows.

(1) Investigation of the operation record

The operation data such as the helium flow rate, the vibration, the rotor temperatures, and the rotational frequencies of the all gas circulators before the reactor scram was checked, and there were no problems on these data. No alarm messages were recorded.

(2) Inspection of the gas circulators

The visual inspection of the all gas circulators was conducted, and abnormality such as failure of a bolt was not observed. Then, the all gas circulators were started-up and vibration, rotor temperatures, rotational frequencies and so on were checked. No abnormal data was found in the test. As the results, these data showed that the integrity of the gas circulator was ensured.

(3) Investigation of electric panels

The electric panels include the breaker panels, the rotational frequency control panels, and the rotational frequency and vibration instrument panels for the PGC. These panels were investigated.

- The breaker panel for PGC

The breaker panels have function to trip the PGCs quickly at a reactor scram. In the reactor scram, the alarm messages of "Breaker panel of PGC (A): Abnormal" and "Trip breaker of PGC (A): Open" were recorded. Thus, the breaker panel for the PGC (A) and other PGC were investigated.

The visual inspection of the relays in the breaker panels was performed without detaching them from the panels, and no flaws were observed. The contact resistances of the relays in the breaker panels were measured, and the contact resistances of two relays

(FV111 and FV161) were higher than other relays. The each relay (FV111 and FV161) monitors a control voltage for trip breaker in A-train and B-train, and send a signal to open the trip breaker. When the voltage is higher than normal limit (i.e., when the function of the breaker panel may not be confirmed), the PGCs are tripped by these breakers.

Then the contact resistances of the two relays were measured for a long-term. The contact resistance of the relay FV111 increased rapidly and the alarm message "Breaker panel of PGC (A): Abnormal" was recorded. In the further measurement, the relay sent a signal to open the trip breaker.

The mechanical malfunction of the trip breaker A-train can cause an opening action of itself. So the action of the trip breaker A-train was investigated by using pseudo-trip-signal. As the results, the abnormal action of the trip breaker was not observed.

- The rotation speed control panel for PGC

The malfunction of a rotational frequency control panel can cause a tripping of the PGC (A). So the rotational frequency control panel was inspected. As the results, the normal operation was confirmed.

The rotation speed and vibration instrument panel did not show abnormality about the rotational frequencies and the vibration for all gas circulators.

(4) The further investigation of the breaker panel for the PGC (A)

The arrangement of the relays in the breaker panels was investigated. The two relays (FV111 and FV161) were placed very close to the adjacent relay, which was always electrically charged and heated-up. The surface temperatures of the two relays (FV111 and FV161) were measured, and they were about 67°C, which was close to the allowable working temperature of 70°C.

Then, the two relays were detached from the breaker panel and the visual inspection was conducted. Change of color and a crack were seen on the surface of the relay (FV111) (see Fig. 3.30), slight change of color was seen on the surface of the relay (FV161). The heat-up test of the relay (FV111) was carried out at the temperature of 60°C for five hours, and at 65°C for three hours. As the result, the malfunction of the relay occurred three times for the former case and five times for the latter case. The arrangement of the relays was checked and relay surface temperature was measured on relays for other breaker panels. The arrangement of the relays for the other breaker panels were acceptable and the relay surface temperatures were low enough.

From the investigation on the operation record, it was concluded that the trip of the PGC (A) was not caused by abnormality in operation.

From the investigation on electric panels, it was concluded that malfunction of the relay (FV111) in the breaker panel for the PGC (A) occurred. The relay (FV111) was placed very close to the adjacent relay that is always electrically charged and heated-up, and its temperature was risen near the allowable working temperature. Therefore, the relay (FV111) was deteriorated and the malfunction occurred. The malfunction of the relay (FV111) caused trip of the PGC (A), which reduced the primary coolant flow rate to the reactor scram level.

Corrective actions were taken as follows:

All voltage monitoring relays for controlling trip breakers for the gas circulators were replaced with new ones. The new relays were arranged so that enough spaces for cooling should be kept between the relays.

The arrangements of all relays in electric panels were checked and confirmed. As a result of detailed investigation, it was confirmed that the trip of the PGC (A) was triggered by malfunction of a relay in a breaker panel for the PGC (A). The relay was affected by the heat of another relay that is located closely and is always electrically charged and heated-up.

As a countermeasure, all similar relays for all gas circulators were replaced with new ones, and relays in the breaker panels were rearranged so that enough spaces for cooling should be kept between the relays.

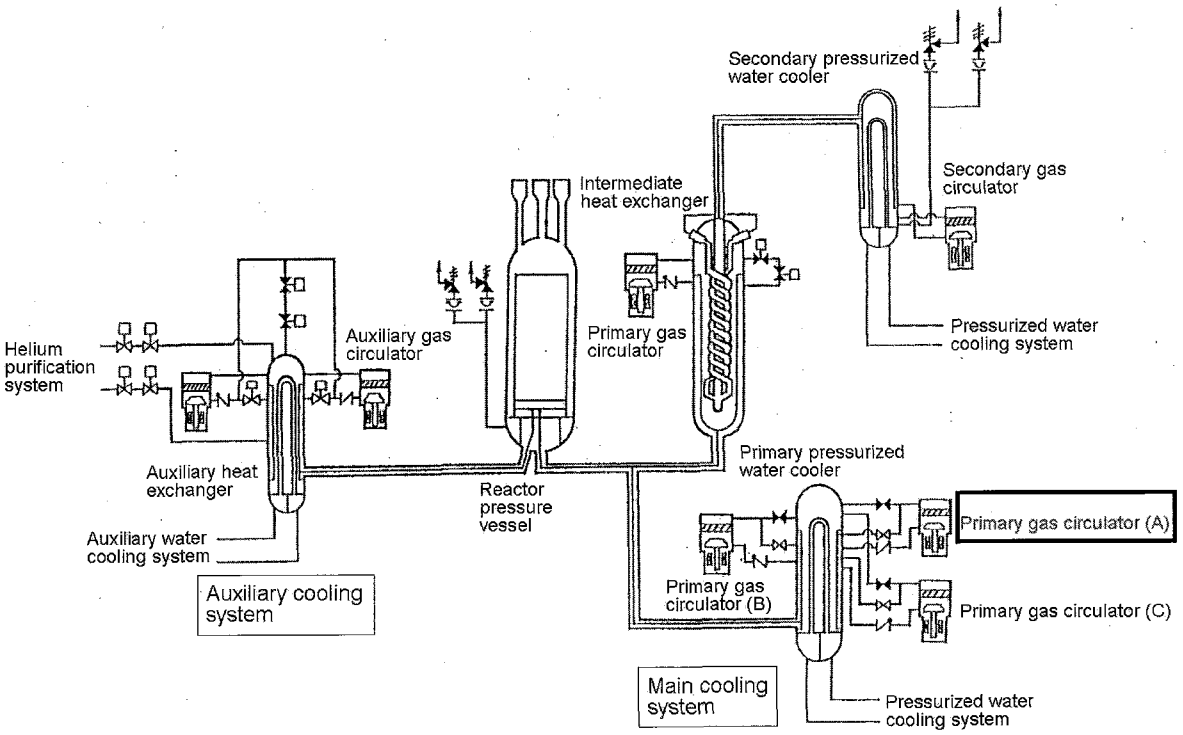

Fig. 3.28 The cooling system of HTTR

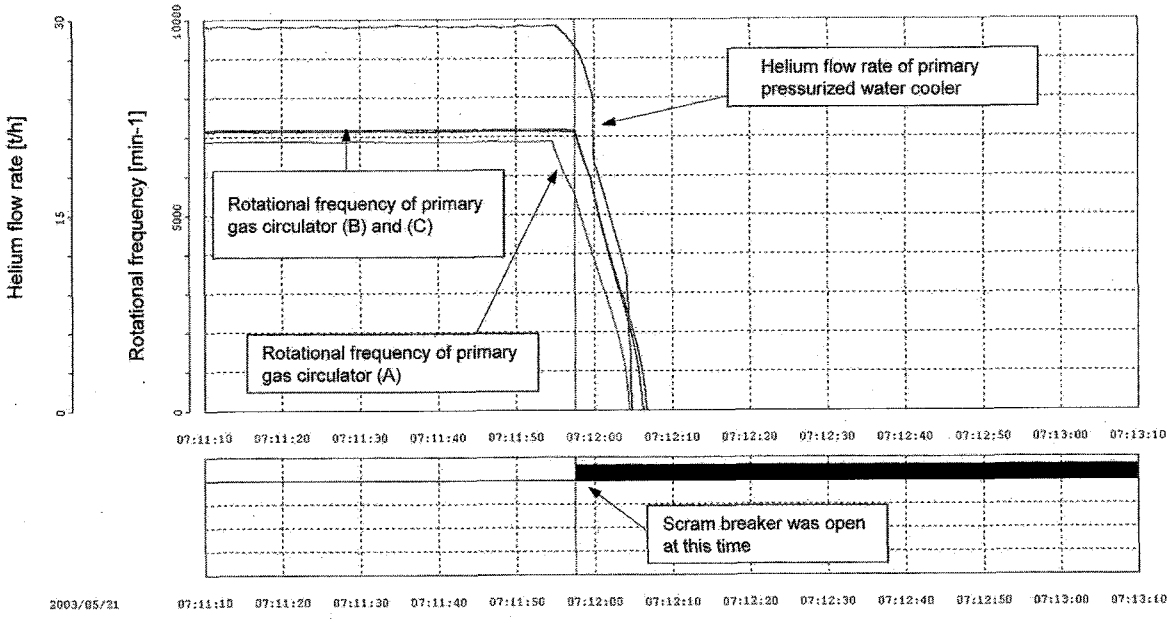

Fig. 3.29 The time variation of helium flow rate and rotational frequency of the PGC at reactor scram

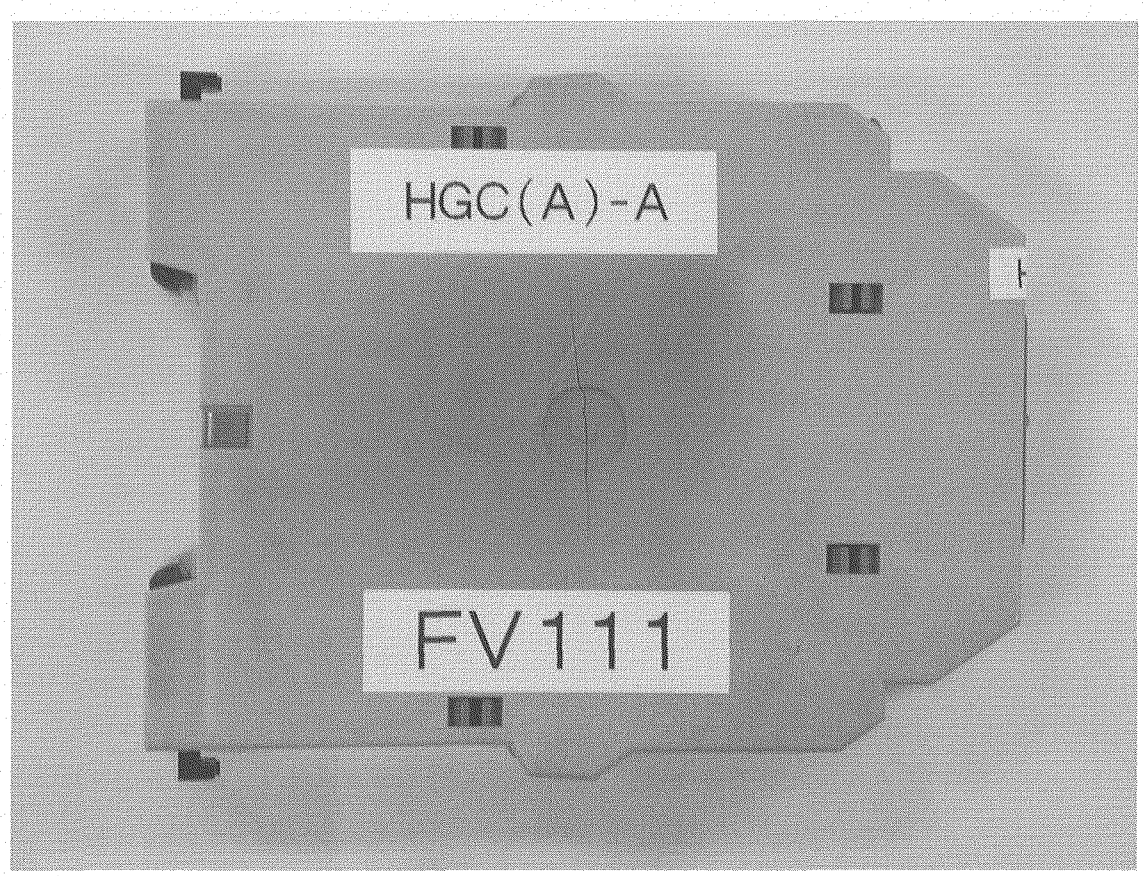

Fig. 3.30 The surface of the relay (FV111)

3.3.3 Reactor scram by operation error caused by an inappropriate expression in operational manual

HTTR scrammed automatically by the scram signal of "Differential of control rod position; Large" during power-up from 8.55MW to 9MW on Feb. 19, 2005 as shown in Fig. 3.31. The reactor scram signal was caused difference in positions of 13 pairs of control rods larger than 20cm above the reactor power 9MW. In HTTR, each pair of control rods is manually withdrawn to the expected critical position, so the difference in control rod position between 13 pair becomes larger than 20cm at an initial critical state.

In the case of reactor power below 9MW, the reactor scram signal of "Differential of control rod position; Large" is permitted to bypass. When the reactor power reached 9MW, the bypass of the reactor scram signal is released automatically. According to the operation manual, when the reactor reached a critical state of 15000cps, the operators must reset the reactor scram signal of "Differential of control rod position; Large" at the local panel. The cause of the reactor scram was investigated as follows:

(1) The investigation of the operation record

The operation data such as the control rod position, the reactor power and the alarm before the reactor automatic scram was checked. As the result, no abnormal data was found and no alarm messages showed abnormality of the reactor operation

(2) Check of the operation manual

The operation manual used in the operation was checked. As the result, it become clear that the operators started power-up without resetting the reactor scram signal of "Differential of control rod position; Large" at the local panel. After that, the next operators (another operators) took over the operation of HTTR from the operators, and they increased the reactor power to 9MW.

From the investigation of the operation manual, it was concluded as follows; The operation manual was changed and the reactivity measurement was added before the operation. However, the operation step after the reactivity measurement was not clear in operation manual, as the result malfunction occurred.

Corrective actions were taken as follows:

(1) All manuals were rechecked. (2) The operators had to take over the plant status and alarm messages to the next operators. (3) The education of the operators was carried out.

As a result of the detailed investigation, it was confirmed that the reactor scram signal of "Differential of control rod position; Large" was caused by an inappropriate expression of operational manual. As a countermeasure, all manuals were reconfirmed.

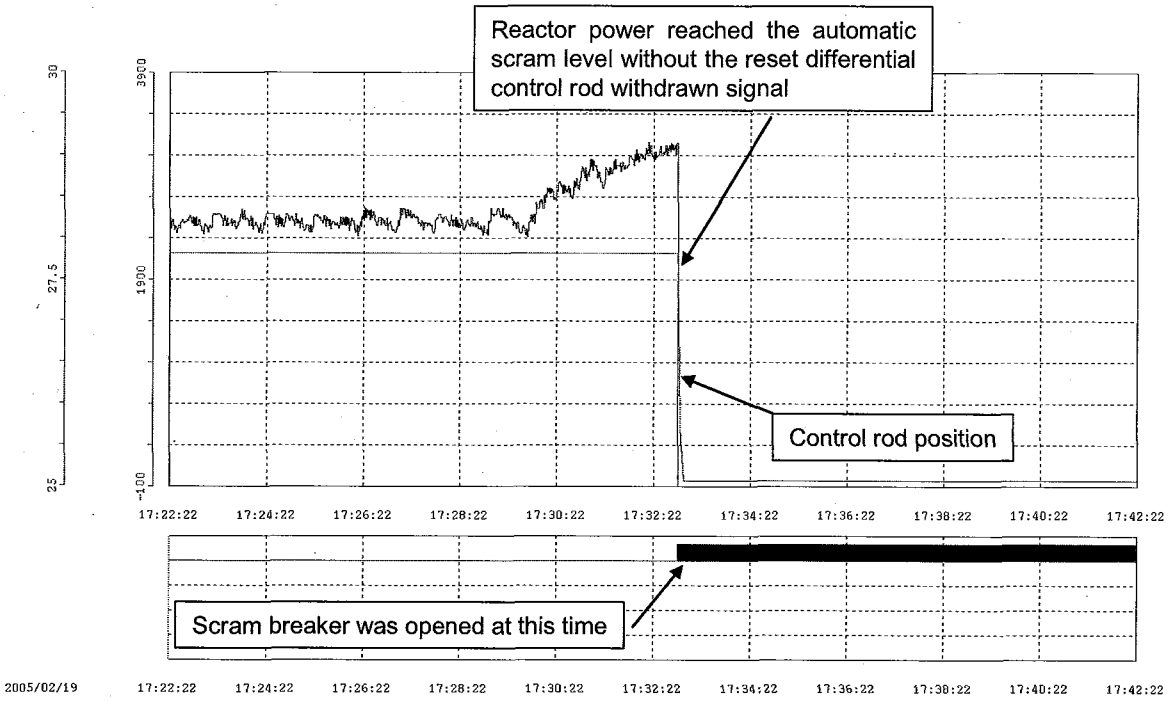

Fig. 3.31 The time transition of reactor scram by the signal "Differential of control rod position; Large"

3.4 Summary

In this section, the operating experiences obtained for five years from the start of the rise-to-power test are described. The description are divided into three categories:

(1) The operating experiences pertaining to new gas cooled reactor design; it is concerned with the design for the next generation HTGR based on the operating experience. In this category, following items are focused:
- ✓ The helium leak rate from the main cooling system
- ✓ The coolant chemistry
- ✓ The core support plate temperature rising
- ✓ The fuel and fission product gases behavior
- ✓ The confirmation of fuel integrity

(2) The operating experiences for the improvement of the performance; it is concerned with corrective action to improve the performances based on rise-to-power test that had carried out to confirm an effective action. In this category, following items are focused:
- ✓ The filter exchange of primary gas circulator
- ✓ The installation of the windshield panels to improve air-cooler performance
- ✓ The inferior of the RSS actuation
- ✓ The contact failure of signal lead wire in WRM

(3) The operating experiences on failure of system and components; it is concerned with the reactor scram and provisions had made for re-start. In this category, following items are focused:
- ✓ The reactor scram by pseudo-signal of vibration sensor
- ✓ The reactor scram by malfunction of a relay for a primary gas circulator
- ✓ The reactor scram by operation error caused by an inappropriate expression of operational manual

There are many inherent experiences for HTGR in these experiences obtained in HTTR. The obtained operating experiences were answer of the missions as to establish HTGR technology and to establish heat utilization system like as hydrogen production system. These are useful and contribute to establishment of future HTGR design and hydrogen production from water using the HTGRs.

In the future, the operating experiences obtained in HTTR will be arranged and informed periodically as useful information for future HTGRs and GFRs.

4. Concluding Remarks

This report describes operating experiences from the start of the rise-to-power test of HTTR. In this report, obtained operating experiences are categorized to the following three types. : (1) Operating experiences related to advanced gas-cooled reactor design, (2) Operating experiences for improvement of the performance, (3) Operating experiences due to fail of system and components.

Obtaining operating experiences are one of the mission of the HTTR project so as to establish HTGR technology and to establish heat utilization system such as hydrogen production system. These are useful and contribute to establishment of future HTGR design and hydrogen production from water using the HTGRs. In the future, useful operating experiences will be stored and arranged periodically.

Acknowledgments

The authors would like to express their appreciation to Mr. Yoshihiro Komori, Mr. Toshio Nakazawa and Mr. Tatsuo Iyoku and Mr. Kiyonobu Yamashita for their useful comments and advices. Moreover the authors would like to express their appreciation to members of HTTR Operation Section, HTTR Reactor Engineering Section and HTTR Project Management section.

References

1) Nakagawa S. et al.: JAERI-Tech 2002-069 "Rise-to-power Test in High Temperature Engineering Test Reactor –Test Progress and Summary of Test Results up to 30MW of Reactor thermal Power–" (2002) (in Japanese).
2) Takamatsu K. et al.: JAERI-Tech 2004-063 "Rise-to-power Test in High Temperature Engineering Test Reactor in the High Temperature Test Operation Mode–Test Progress and Summary of Test Results up to 30MW of Reactor thermal Power–" (2004) (in Japanese).
3) Saito S. et al.: JAERI-1332 "Design of High Temperature Engineering Test Reactor (HTTR)" (1994).
4) Ueta S. et al.: JAERI-Tech 2003-025 "An Investigation of Fuel and Fission Product Behavior in Rise-to-power Test of HTTR (No. 2: Result Up to 30MW Operation)" (2003) (in Japanese).
5) Tochio D. et al. "Evaluation of Fuel Temperature on High temperature Test Operation at High Temperature Gas-Cooled Reactor 'HTTR'," Trans At. Energy Soc. Japan, 5(1),

pp.57-67 (2006) (in Japanese).

6) Fujimoto N. et al.: JAERI-Tech 2001-090 "Cause and Countermeasure for Heat Up of HTTR Core Support Plate at Power Rise Test" (2001) (in Japanese).

7) Furusawa T. et al.: JAERI-Tech 2004-024 "Replacement of the Filter for Primary Helium Circulators of the HTTR" (2004) (in Japanese).

8) Hamamoto S. et al.: JAEA Technology 2006-030 "Report of Investigation on Malfunction of Reserved Shutdown System in HTTR" (2006) (in Japanese).

9) Hirato Y. et al.: JAERI-Tech 2004-037 "Investigation of Automatic Shutdown of HTTR on May 21st, 2003" (2003) (in Japanese).

10) Takamatsu K.: JAERI-Tech 2003-062 "Findings of the Reactor Automatic Shutdown Caused by a Signal of "Primary Coolant Flow Rate of the PPWC: Low" in HTTR" (2003) (in Japanese).

国際単位系（SI）

表１．SI 基本単位

基本量	SI 基本単位	
	名称	記号
長さ	メートル	m
質量	キログラム	kg
時間	秒	s
電流	アンペア	A
熱力学温度	ケルビン	K
物質量	モル	mol
光度	カンデラ	cd

表２．基本単位を用いて表されるSI組立単位の例

組立量	SI 基本単位	
	名称	記号
面積	平方メートル	m^2
体積	立法メートル	m^3
速さ，速度	メートル毎秒	m/s
加速度	メートル毎秒毎秒	m/s^2
波数	毎メートル	m^{-1}
密度（質量密度）	キログラム毎立法メートル	kg/m^3
質量体積（比体積）	立法メートル毎キログラム	m^3/kg
電流密度	アンペア毎平方メートル	A/m^2
磁界の強さ	アンペア毎メートル	A/m
（物質量の）濃度	モル毎立方メートル	mol/m^3
輝度	カンデラ毎平方メートル	cd/m^2
屈折率	（数の）1	1

表５．SI 接頭語

乗数	接頭語	記号	乗数	接頭語	記号
10^{24}	ヨタ	Y	10^{-1}	デシ	d
10^{21}	ゼタ	Z	10^{-2}	センチ	c
10^{18}	エクサ	E	10^{-3}	ミリ	m
10^{15}	ペタ	P	10^{-6}	マイクロ	μ
10^{12}	テラ	T	10^{-9}	ナノ	n
10^{9}	ギガ	G	10^{-12}	ピコ	p
10^{6}	メガ	M	10^{-15}	フェムト	f
10^{3}	キロ	k	10^{-18}	アト	a
10^{2}	ヘクト	h	10^{-21}	ゼプト	z
10^{1}	デカ	da	10^{-24}	ヨクト	y

表３．固有の名称とその独自の記号で表されるSI組立単位

組立量	SI 組立単位			
	名称	記号	他のSI単位による表し方	SI基本単位による表し方
平面角	ラジアン(a)	rad		$m \cdot m^{-1}=1$(b)
立体角	ステラジアン(a)	sr(c)		$m^2 \cdot m^{-2}=1$(b)
周波数	ヘルツ	Hz		s^{-1}
力	ニュートン	N		$m \cdot kg \cdot s^{-2}$
圧力，応力	パスカル	Pa	N/m^2	$m^{-1} \cdot kg \cdot s^{-2}$
エネルギー，仕事，熱量	ジュール	J	$N \cdot m$	$m^2 \cdot kg \cdot s^{-2}$
工率，放射束	ワット	W	J/s	$m^2 \cdot kg \cdot s^{-3}$
電荷，電気量	クーロン	C		$s \cdot A$
電位差（電圧），起電力	ボルト	V	W/A	$m^2 \cdot kg \cdot s^{-3} \cdot A^{-1}$
静電容量	ファラド	F	C/V	$m^{-2} \cdot kg^{-1} \cdot s^4 \cdot A^2$
電気抵抗	オーム	Ω	V/A	$m^2 \cdot kg \cdot s^{-3} \cdot A^{-2}$
コンダクタンス	ジーメンス	S	A/V	$m^{-2} \cdot kg^{-1} \cdot s^3 \cdot A^2$
磁束	ウエーバ	Wb	$V \cdot s$	$m^2 \cdot kg \cdot s^{-2} \cdot A^{-1}$
磁束密度	テスラ	T	Wb/m^2	$kg \cdot s^{-2} \cdot A^{-1}$
インダクタンス	ヘンリー	H	Wb/A	$m^2 \cdot kg \cdot s^{-2} \cdot A^{-2}$
セルシウス温度	セルシウス度(d)	℃		K
光束	ルーメン	lm	$cd \cdot sr$(c)	$m^2 \cdot m^{-2} \cdot cd=cd$
照度	ルクス	lx	lm/m^2	$m^2 \cdot m^{-4} \cdot cd=m^{-2} \cdot cd$
（放射性核種の）放射能	ベクレル	Bq		s^{-1}
吸収線量，質量エネルギー分与，カーマ	グレイ	Gy	J/kg	$m^2 \cdot s^{-2}$
線量当量，周辺線量当量，方向性線量当量，個人線量当量，組織線量当	シーベルト	Sv	J/kg	$m^2 \cdot s^{-2}$

(a) ラジアン及びステラジアンの使用は、同じ次元であっても異なった性質をもった量を区別するときの組立単位の表し方として利点がある。組立単位を形作るときのいくつかの用例は表４に示されている。
(b) 実際には、使用する時には記号rad及びsrが用いられるが、習慣として組立単位としての記号“１”は明示されない。
(c) 測光学では、ステラジアンの名称と記号srを単位の表し方の中にそのまま維持している。
(d) この単位は、例としてミリセルシウス度m℃のようにSI接頭語を伴って用いても良い。

表４．単位の中に固有の名称とその独自の記号を含むSI組立単位の例

組立量	SI 組立単位		
	名称	記号	SI 基本単位による表し方
粘度	パスカル秒	Pa・s	$m^{-1} \cdot kg \cdot s^{-1}$
力のモーメント	ニュートンメートル	N・m	$m^2 \cdot kg \cdot s^{-2}$
表面張力	ニュートン毎メートル	N/m	$kg \cdot s^{-2}$
角速度	ラジアン毎秒	rad/s	$m \cdot m^{-1} \cdot s^{-1}=s^{-1}$
角加速度	ラジアン毎平方秒	rad/s^2	$m \cdot m^{-1} \cdot s^{-2}=s^{-2}$
熱流密度，放射照度	ワット毎平方メートル	W/m^2	$kg \cdot s^{-3}$
熱容量，エントロピー	ジュール毎ケルビン	J/K	$m^2 \cdot kg \cdot s^{-2} \cdot K^{-1}$
質量熱容量（比熱容量），質量エントロピー	ジュール毎キログラム毎ケルビン	J/(kg・K)	$m^2 \cdot s^{-2} \cdot K^{-1}$
質量エネルギー（比エネルギー）	ジュール毎キログラム	J/kg	$m^2 \cdot s^{-2} \cdot K^{-1}$
熱伝導率	ワット毎メートル毎ケルビン	W/(m・K)	$m \cdot kg \cdot s^{-3} \cdot K^{-1}$
体積エネルギー	ジュール毎立方メートル	J/m^3	$m^{-1} \cdot kg \cdot s^{-2}$
電界の強さ	ボルト毎メートル	V/m	$m \cdot kg \cdot s^{-3} \cdot A^{-1}$
体積電荷	クーロン毎立方メートル	C/m^3	$m^{-3} \cdot s \cdot A$
電気変位	クーロン毎平方メートル	C/m^2	$m^{-2} \cdot s \cdot A$
誘電率	ファラド毎メートル	F/m	$m^{-3} \cdot kg^{-1} \cdot s^4 \cdot A^2$
透磁率	ヘンリー毎メートル	H/m	$m \cdot kg \cdot s^{-2} \cdot A^{-2}$
モルエネルギー	ジュール毎モル	J/mol	$m^2 \cdot kg \cdot s^{-2} \cdot mol^{-1}$
モルエントロピー，モル熱容量	ジュール毎モル毎ケルビン	J/(mol・K)	$m^2 \cdot kg \cdot s^{-2} \cdot K^{-1} \cdot mol^{-1}$
照射線量（X線及びγ線）	クーロン毎キログラム	C/kg	$kg^{-1} \cdot s \cdot A$
吸収線量率	グレイ毎秒	Gy/s	$m^2 \cdot s^{-3}$
放射強度	ワット毎ステラジアン	W/sr	$m^4 \cdot m^{-2} \cdot kg \cdot s^{-3}=m^2 \cdot kg \cdot s^{-3}$
放射輝度	ワット毎平方メートル毎ステラジアン	$W/(m^2 \cdot sr)$	$m^2 \cdot m^{-2} \cdot kg \cdot s^{-3}=kg \cdot s^{-3}$

表６．国際単位系と併用されるが国際単位系に属さない単位

名称	記号	SI 単位による値
分	min	1 min=60s
時	h	1h =60 min=3600 s
日	d	1 d=24 h=86400 s
度	°	1°=(π/180) rad
分	’	1’=(1/60)°=(π/10800) rad
秒	”	1”=(1/60)’=(π/648000) rad
リットル	l、L	1l=1 $dm^3=10^{-3}m^3$
トン	t	$1t=10^3$ kg
ネーパ	Np	1Np=1
ベル	B	1B=(1/2)ln10(Np)

表７．国際単位系と併用されこれに属さない単位で SI単位で表される数値が実験的に得られるもの

名称	記号	SI 単位であらわされる数値
電子ボルト	eV	$1eV=1.60217733(49) \times 10^{-19}J$
統一原子質量単位	u	$1u=1.6605402(10) \times 10^{-27}kg$
天文単位	ua	$1ua=1.49597870691(30) \times 10^{11}m$

表８．国際単位系に属さないが国際単位系と 併用されるその他の単位

名称	記号	SI 単位であらわされる数値
海里		1海里=1852m
ノット		1ノット=1海里毎時=(1852/3600)m/s
アール	a	1a=1 $dam^2=10^2m^2$
ヘクタール	ha	1ha=1 $hm^2=10^4m^2$
バール	bar	1bar=0.1MPa=100kPa=1000hPa=10^5Pa
オングストローム	Å	1 Å=0.1nm=10^{-10}m
バーン	b	1b=100$fm^2=10^{-28}m^2$

表９．固有の名称を含むCGS組立単位

名称	記号	SI 単位であらわされる数値
エルグ	erg	$1 erg=10^{-7}$ J
ダイン	dyn	$1 dyn=10^{-5}$N
ポアズ	P	1 P=1 dyn・s/cm^2=0.1Pa・s
ストークス	St	1 St =1$cm^2/s=10^{-4}m^2/s$
ガウス	G	1 G ^10^{-4}T
エルステッド	Oe	1 Oe ^(1000/4π)A/m
マクスウェル	Mx	1 Mx ^10^{-8}Wb
スチルブ	sb	1 sb =1$cd/cm^2=10^4cd/m^2$
ホト	ph	1 ph=10^4lx
ガル	Gal	1 Gal =1$cm/s^2=10^{-2}m/s^2$

表10．国際単位に属さないその他の単位の例

名称	記号	SI 単位であらわされる数値
キュリー	Ci	$1 Ci=3.7 \times 10^{10}Bq$
レントゲン	R	$1 R = 2.58 \times 10^{-4}C/kg$
ラド	rad	$1 rad=1cGy=10^{-2}Gy$
レム	rem	$1 rem=1 cSv=10^{-2}Sv$
X線単位		$1X unit=1.002 \times 10^{-4}nm$
ガンマ	γ	$1\gamma=1 nT=10^{-9}T$
ジャンスキー	Jy	$1 Jy=10^{-26}W \cdot m^{-2} \cdot Hz^{-1}$
フェルミ		$1 fermi=1 fm=10^{-15}m$
メートル系カラット		1 metric carat = 200 mg = 2×10^{-4}kg
トル	Torr	1 Torr = (101 325/760) Pa
標準大気圧	atm	1 atm = 101 325 Pa
カロリー	cal	
ミクロン	μ	$1 \mu=1\mu m=10^{-6}m$

（第７版，1998年改訂）